A TRANSFORMER-BASED POLY-PHASE NETWORK FOR ULTRA-BROADBAND QUADRATURE SIGNAL GENERATION

A Thesis
Presented to
The Academic Faculty

by

Jongseok Park

In Partial Fulfillment
of the Requirements for the Degree
Masters in the
School of Electrical and Computer Engineering

Georgia Institute of Technology
December 2016

A TRANSFORMER-BASED POLY-PHASE NETWORK FOR ULTRA-BROADBAND QUADRATURE SIGNAL GENERATION

Approved by:

Dr. Hua Wang, Advisor
School of Electrical and Computer Engineering
Georgia Institute of Technology

Dr. Muhannad S. Bakir
School of Electrical and Computer Engineering
Georgia Institute of Technology

Dr. John D. Cressler
School of Electrical and Computer Engineering
Georgia Institute of Technology

Date Approved: 12/7/2016

TABLE OF CONTENTS

LIST OF TABLES

LIST OF FIGURES

SUMMARY

This paper presents a transformer-based poly-phase network to generate fully differential quadrature signals with low loss, compact area, and high-precision magnitude and phase balance over an ultra-wide bandwidth. A fully differential high-coupling 8-port folded transformer-based quadrature hybrid serves as the basic building block for the poly-phase unit stage to achieve significant size reduction and low loss. Multiple poly-phase unit stages can be cascaded to form the multistage poly-phase network to substantially extend the quadrature signal generation bandwidth. The designs of the high-coupling transformer-based quadrature hybrid, the poly-phase unit stage, and the multistage transformer-based poly-phase network are presented with the closed-form design equations in this paper. As a proof-of-concept design, a 3-stage transformer-based poly-phase network is implemented in a standard 65 nm bulk CMOS process with a core area of 772 μm 925 μm. Measurement results of this poly-phase network over 3 independent samples demonstrate that the output In-Phase and Quadrature (I/Q) magnitude mismatch is less than 1 dB from 2.8 GHz to 21.8 GHz with a passive loss of 3.65 dB at 6.4 GHz. The measured output I/Q phase error is less than 10° from 0.1 GHz to 24 GHz. The effective Image Rejection Ratio (IRR) based on the measured I/Q balancing is more than 30 dB from 3.7 GHz to 22.5 GHz. The 3-stage transformer-based poly-phase network design achieves high-quality quadrature signal generation over a first-ever one-decade bandwidth together with low-loss and compact area.

CHAPTER I

INTRODUCTION

Quadrature signal generation plays a critical role in many RF, mm-wave, and mixed-signal circuits and systems. Popular circuit block examples include In-Phase/Quadrature (I/Q) vector modulator-based phase rotator [1], Doherty power amplifier [2], and balanced amplifier [3], all of which employ the quadrature signal generation blocks as their key components. As the system examples, Hartley and Weaver receivers [4] require quadrature Local Oscillator (LO) signals and/or quadrature signal combining networks for image rejections. Moreover, in many wireless communication and radar systems, the beam former structures, e.g., Butler matrix [5], phased-array transceiver [6], and circular/elliptical polarized antenna [7], also rely on quadrature signal generation. Passive networks are commonly used for quadrature generation due to their superior linearity, zero power consumption, and frequency scalability. Passive quadrature generation networks are often evaluated by their passive loss, bandwidth, I/Q magnitude and phase balance, and robustness against the process variations. The RC-CR pairs and RC-CR poly-phase filters have been widely used due to their simplicity [4]. However, the RC-CR pairs suffer from inherent signal loss and narrow bandwidth, fundamentally due to the resistive components in the signal paths. Moreover, this RC-CR based approach is sensitive to the source impedances and load terminations, particularly limiting its use at mm-wave frequencies. By cascading multiple RC-CR stages, the RC-CR poly-phase networks can extend the quadrature generation bandwidth and improve the process variation robustness but at the expense of further signal loss [8], posing a direct trade-off between signal loss and bandwidth. On the other hand, transmission line couplers [3] can generate I/Q output signals with input/output matching at RF and mm-wave frequencies. However, the required transmission lines often occupy a substantial chip area, making on-chip integration challenging. In addition, L-C resonance based quadrature all-pass filter is also reported for

I/Q generation [9]. Transformer-based quadrature generations are recently gaining an increasing interest. A one-stage singled-ended transformer-based 3 dB quadrature hybrid with its magnetic coupling coefficient k of 0.707 is reported at RF frequency (2 GHz) [10] and is later extended to mm-wave frequencies [11], [5]. This scheme offers low loss, high precision I/Q balancing, input/output matching, and a compact footprint even at the low RF frequency range. To further reduce the area, a fully differential folded transformer-based 3 dB quadrature hybrid is recently reported [12], which generates fully differential quadrature signals within only one inductor footprint by exploiting magnetic coupling enhancement of the differential mode operation. Transformer-based quadrature generation networks typically achieve 20% fractional bandwidth mainly limited by the I/Q magnitude mismatches. Although this bandwidth can be sufficient for many narrow-band applications, it cannot support wideband systems, such as broadband radars [13], hyperspectral imagers [14], or wideband antenna mode formers [15]. To address these challenges, we propose a transformer-based poly-phase network to suppress I/Q magnitude/phase mismatches and achieve ultra-broadband operation with low loss and a compact form factor [16]. This paper presents the complete circuit analysis, design equations, full simulation results, and extended measurement results to demonstrate the proposed transformer-based poly-phase network. In Section II, the circuit analysis, design equations, and graphic summary of the simulation results for high-coupling transformer-based quadrature hybrid are presented. Compared with the conventional quadrature hybrid design [10], it achieves a smaller required inductance and a wider bandwidth. The high-coupling transformer-based quadrature hybrid is then extended to a fully differential 8-port folded transformer design, which serves as the building block for the poly-phase unit stage. Section III shows the complete theoretical analysis of the multi-stage transformer-based poly-phase network. In particular, the resulting I/Q magnitude mismatch versus the number of poly-phase stages is thoroughly presented with the analytical design equations and compared with 3-D electromagnetic (EM) simulation results. These results demonstrate the fundamental basis

of why cascading multiple transformer-based poly-phase unit stages can suppress the I/Q magnitude mismatch and substantially extend the bandwidth. As a proof-of-concept demonstration, in Section IV, we present a 3-stage transformer-based poly-phase network design example implemented in a 65 nm CMOS process with design details and simulation results. In Section V, complete measurement results on 3 independent samples are presented to demonstrate the robustness and repeatability of the proposed transformer-based poly-phase network.

CHAPTER II

TRANSFORMER-BASED QUADRATURE SIGNAL GENERATION

The schematic of the transformer-based quadrature hybrid [10] is shown in Fig. 1(a). Here, we will perform circuit analysis on this hybrid structure. We will also derive the complete and general design equations for an arbitrary coupling coefficient k, based on which, we will propose the high-coupling transformer quadrature hybrid.

When driven only at the input port (IN), this transformer-based network utilizes both inductive and capacitive couplings to achieve matched quadrature output signals at the through port (THRU, -90°) and the coupled port (CPL, 0°), shown in Fig. 1(a). The inductive coupling coefficient k_L and the capacitive coupling coefficient k_C are defined in equations (1) and (2), respectively. L_M and C_M indicate the mutual inductance and mutual capacitance, and the quantity C is defined as C_M+C_G.

$$k_L = \frac{L_M}{L} \tag{1}$$

$$k_C = \frac{C_M}{\sqrt{(C_G + C_M)(C_G + C_M)}} = \frac{C_M}{C} \tag{2}$$

For the even-mode operation ($V_{ex1}=V_{ex2}=V_0$), a virtual open-circuit condition exists along the symmetric line in Fig. 1(a), and a positive magnetic coupling ($i_1=i_2$) is achieved. Thus, the equivalent even-mode half-circuit consists of an C-L-C pi-network with the even-mode inductance $L_e=L(1+k_L)$ and the even-mode capacitance $C_e=C(1-k_C)$, shown in Fig. 1(b). The even-mode characteristic impedance Z_{0e} and propagation velocity v_e are given in (3) and (4), and the even-mode voltages at all the nodes (V_{1e}-V_{4e}) are shown in (5) and (6). Note that V_{3e} and V_{4e} are the input and output voltages for the other and identical even-mode half circuit, which is not shown in Fig. 1(b).

$$Z_{0e} = \sqrt{\frac{L_e}{C_e}} = \sqrt{\frac{L(1 + k_L)}{C(1 - k_C)}} \tag{3}$$

$$v_e = \frac{1}{\sqrt{L_e C_e}} = \frac{1}{\sqrt{L(1+k_L)C(1-k_C)}} \tag{4}$$

$$V_{1e} = V_{3e} = V_0 \frac{(\frac{1}{SC_e} // Z_0 + SL_e) // \frac{1}{SC_e}}{Z_0 + (\frac{1}{SC_e} // Z_0 + SL_e) // \frac{1}{SC_e}} \tag{5}$$

$$V_{2e} = V_{4e} = V_{1e} \frac{\frac{1}{SC_e} // Z_0}{\frac{1}{SC_e} // Z_0 + SL_e} \tag{6}$$

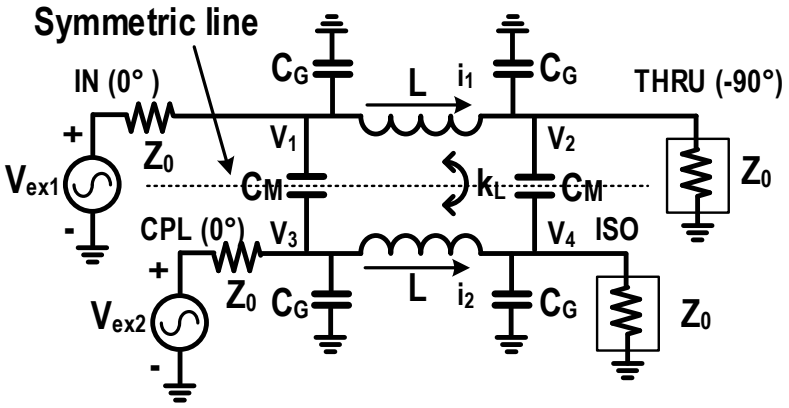

(a) Transformer-based quadrature generation network

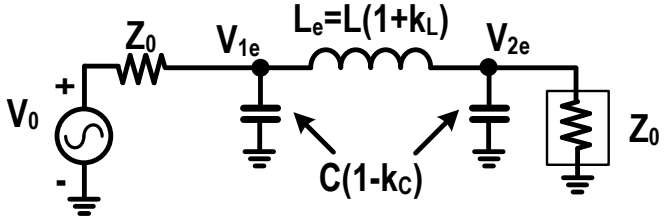

(b) Even-mode half-circuit ($V_{ex1}=V_{ex2}=V_0$)

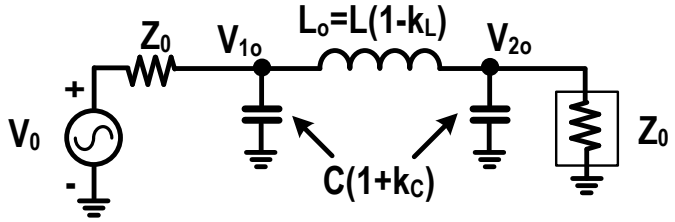

(c) Odd-mode half-circuit ($V_{ex1}=-V_{ex2}=V_0$)

Fig. 1. The (a) transformer-based quadrature hybrid schematic and (b) its even-mode half-circuit and (c) odd-mode half-circuit.

In the odd-mode operation (V_{ex1}=-V_{ex2}=V_0), a virtual ground is established along the symmetric line in Fig. 1(a), and the magnetic coupling (i_1=-i_2) is negative. Therefore, the odd-mode inductance L_o equals $L(1-k_L)$, and the odd-mode capacitance C_o equals $C(1+k_C)$, shown in the odd-mode half-circuit in Fig. 1(c). The odd-mode characteristic impedance Z_{0o}, propagation velocity v_o, and the voltages at all the nodes (V_{1o}-V_{4o}) are shown in equations (7)-(10). Note that V_{3o} and V_{4o} are the input and output voltages for the other and identical odd-mode half circuit, which is not shown in Fig. 1(c).

$$Z_{0o} = \sqrt{\frac{L_o}{C_o}} = \sqrt{\frac{L(1-k_L)}{C(1+k_C)}} \tag{7}$$

$$v_o = \frac{1}{\sqrt{L_o C_o}} = \frac{1}{\sqrt{L(1-k_L)C(1+k_C)}} \tag{8}$$

$$V_{1o} = -V_{3o} = V_0 \frac{(\frac{1}{SC_o} // Z_0 + SL_o) // \frac{1}{SC_o}}{Z_0 + (\frac{1}{SC_o} // Z_0 + SL_o) // \frac{1}{SC_o}} \tag{9}$$

$$V_{2o} = -V_{4o} = V_{1o} \frac{\frac{1}{SC_o} // Z_0}{\frac{1}{SC_o} // Z_0 + SL_o} \tag{10}$$

The transformer-based quadrature hybrid can be treated as a one-section synthetic coupled transmission line. For the desired transverse electromagnetic mode (TEM) propagation, the even-mode and odd-mode propagation velocities should equal to avoid dispersions [3]. Therefore, the capacitive coupling and the inductive coupling should be identical (k_C=k_L=k) based on (4) and (8). Therefore, the 4-port S-parameters of the transformer-based quadrature hybrid can be obtained by the equations (11)-(15). Due to the symmetry, Z_{in} is the input impedance of any port with the other 3 ports loaded with Z_0 defined in (19).

$$S_{11} = S_{22} = S_{33} = S_{44} = \frac{Z_{in} - Z_0}{Z_{in} + Z_0} \tag{11}$$

$$Z_{in} = Z_0 \frac{(V_{1e} + V_{1o})}{(2V_0 - V_{1e} - V_{1o})} \tag{12}$$

$$S_{21} = S_{12} = (V_{2e} + V_{2o})/V_0 \tag{13}$$

$$S_{31} = S_{13} = V_{3e} + V_{3o} = (V_{1e} - V_{1o})/\, V_0 \tag{14}$$

$$S_{41} = S_{14} = (V_{4e} + V_{4o})/V_0 \tag{15}$$

To achieve quadrature signal generation, the equivalent coupled transmission line should behave as a quarter-wave line at the frequency $\omega_{\lambda/4}$ [3]. At this frequency, assume that the IN-port is excited by a source voltage of $2V_{IN}(\omega_{\lambda/4})$, the CPL-port and THRU-port outputs are given as

$$\frac{V_{CPL}(\omega_{\lambda/4})}{V_{IN}(\omega_{\lambda/4})} = \frac{Z_{0e} - Z_{0o}}{Z_{0e} + Z_{0o}} = k \tag{16}$$

$$\frac{V_{THRU}(\omega_{\lambda/4})}{V_{IN}\,(\omega_{\lambda/4})} = -j\sqrt{1 - k^2}. \tag{17}$$

Therefore, the excitation at the IN-port will result in quadrature signals at the CPL-port and THRU-port. The complete design parameters for a transformer-based quadrature generation network can be uniquely specified by the equations (18)-(20) at the frequency $\omega_{\lambda/4}$.

$$\frac{C_M}{C} = k \tag{18}$$

$$Z_0 = \sqrt{Z_{0e}Z_{0o}} = \sqrt{\frac{L}{C}} \tag{19}$$

$$\omega_{\lambda/4} = \frac{1}{\sqrt{LC(1 - k^2)}} \tag{20}$$

Based on (16)-(20), it is clear that the coupling coefficient k is an essential design parameter for the transformer-based quadrature hybrid, since it determines the output

magnitudes of the CPL-port and the THRU-port as well as the required inductance and capacitance at the frequency $\omega_{\lambda/4}$.

It is of particular interest to investigate the transformer-based quadrature hybrid with equal output amplitudes and a 90° phase difference at the CPL-port and the THRU-port at the frequency $\omega_{\lambda/4}$. Based on (16) and (17), the coupling coefficient k should be 0.707 to achieve such 3 dB quadrature hybrid at $\omega_{\lambda/4}$. The result of such a special case matches the design guidelines presented in [10]. However, the requirement of k=0.707 directly limits the geometric design freedom and the footprint of the transformer structure.

To address this limitation, we will next propose and demonstrate a 3 dB transformer quadrature hybrid using a high-coupling (high-k) transformer. This approach obviates the need of enforcing k=0.707 and allows a high-k transformer with a more compact footprint and lower loss. Based on (16) and (17), for k>0.707, the V_{CPL} magnitude |k| is larger than the V_{THRU} magnitude $(|1-k^2|)^{1/2}$ at $\omega_{\lambda/4}$. On the other hand, at a very low frequency (e.g., near dc), it is clear that V_{CPL}=0 (open-circuit) and $V_{THRU}=V_{IN}(\omega_{\lambda/4})$ (short-circuit) based on Fig. 1(a). Therefore, if we design a transformer-based 3 dB quadrature hybrid with k>0.707, there exists at least one frequency value ω_0 between dc to $\omega_{\lambda/4}$, at which the 3 dB quadrature hybrid relationship ($|V_{CPL}|=|V_{THRU}|$) is achieved. On the other hand, if k is smaller than 0.707, then $|V_{CPL}|<|V_{THRU}|$ at both dc and $\omega_{\lambda/4}$. The existence of the frequency value ω_0 for 3 dB quadrature hybrid relationship is not mathematically guaranteed from dc to $\omega_{\lambda/4}$. To illustrate this high-k design concept, Figure 2 shows the calculated magnitude/phase responses based on (11)-(15) for a transformer-based 3 dB quadrature hybrid design with k=0.82, Z_0=50 Ω, $\omega_{\lambda/4}$=1, and L=87, where the frequency and inductance are normalized values. With k=0.82, the CPL-port signal ($|V_{CPL}|=|k|=0.82$) is greater than the THRU-port signal ($|V_{THRU}|=(|1-k^2|)^{1/2}=0.57$) at $\omega_{\lambda/4}$=1. The 3 dB quadrature hybrid relationship ($|V_{CPL}|=|V_{THRU}|$) is achieved at ω_0=0.54 (Fig. 2(a)). Note that the return loss is more than 15 dB from dc up to a normalized frequency of 1.25. The phase mismatch is lower than 3° up to $\omega_{\lambda/4}$=1, and is only 10° at the normalized frequency of 1.33. In

contrast, a conventional 3 dB quadrature hybrid with k=0.707 at the frequency ω_0=0.54 requires an inductor L of 130, which is 1.49× larger than our high-k transformer design (k=0.82 and L=87). Therefore, our high-k design allows a significant transformer size reduction.

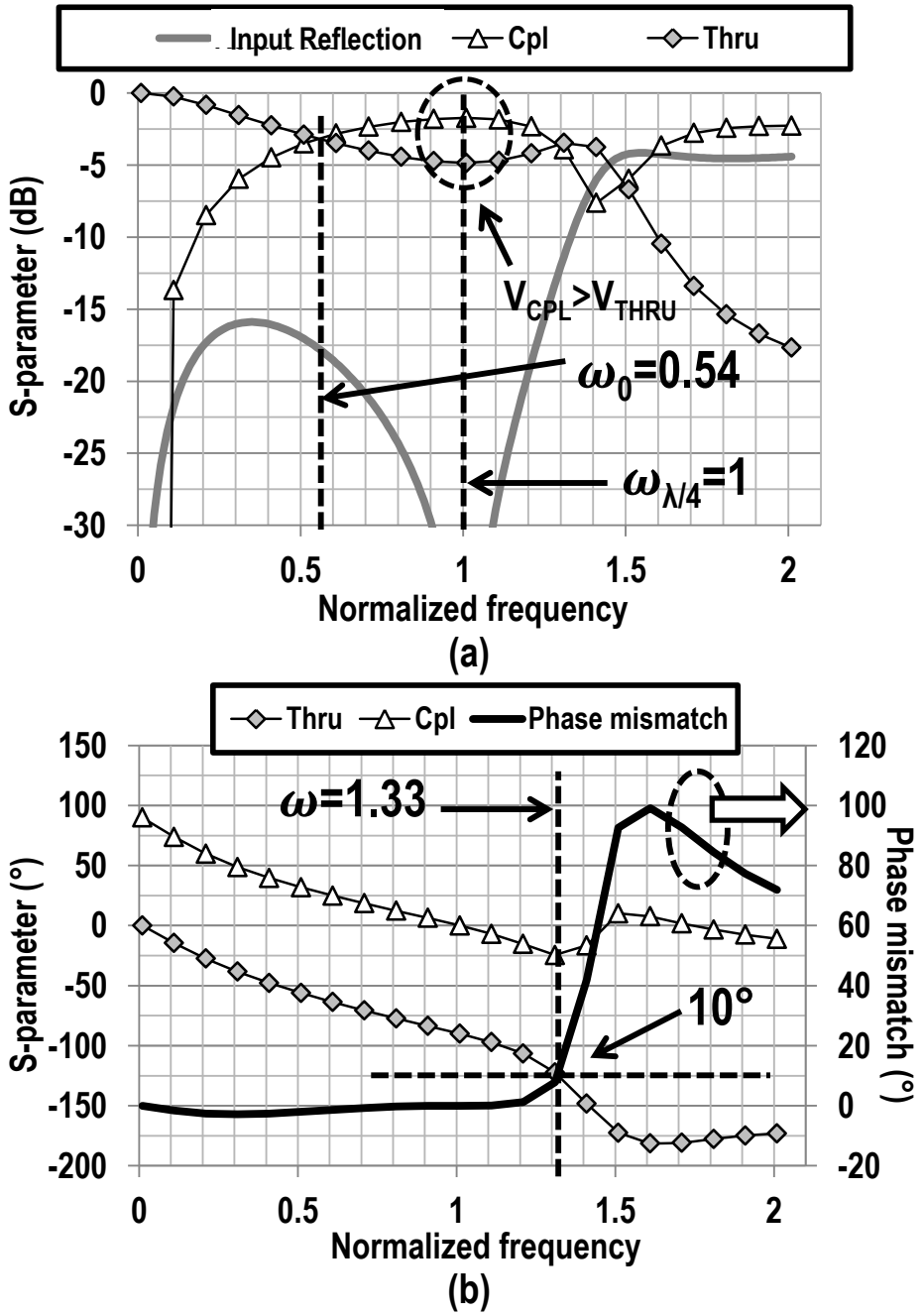

Fig. 2. The simulated (a) magnitude and (b) phase responses for the high-k transformer 3 dB quadrature hybrid with k=0.82 and Z_0=50 Ω.

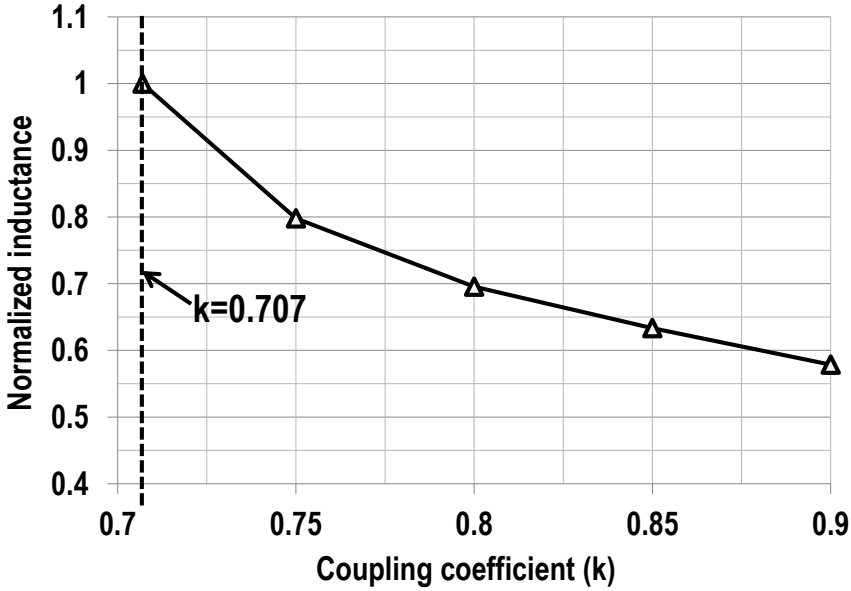

Fig. 3. The calculated inductance for different coupling k to achieve 3 dB quadrature hybrid at a fixed given frequency ω_0. The inductance value is normalized to the conventional hybrid design with k=0.707.

Figure 3 summarizes the normalized inductance values to achieve the 3 dB quadrature hybrid operation at a given frequency ω_0 for different coupling k values. The required inductance values are normalized to the value in the conventional quadrature hybrid design with k=0.707. As the coupling coefficient k increases, the required inductance decreases, achieving a substantial transformer size reduction. Besides size reduction, our proposed high-k transformer quadrature hybrid also enables wideband operation. To demonstrate this aspect, we will analyze the output I/Q magnitude/phase mismatches versus frequency as follows. Assuming the port 1 is the input port of the quadrature hybrid (Fig. 1(a)), based on the 4-port S-parameters design equations of the transformer quadrature hybrid (11)-(15), the magnitude and phase responses of the CPL-port (S_{31}) and the THRU-port (S_{21}) can be derived and shown below.

$$S_{21}(s) = \frac{2A(s)Z_0}{A(s)^2 - B(s)^2} \tag{21}$$

$$S_{31}(s) = \frac{2B(s)C(s) + 2A(s)D(s)}{A(s)^2 - B(s)^2} \tag{22}$$

$$A(s) = s^3L^2C(1-k^2) + 2Z_0s^2LC(1-k^2) + 3sL + 2Z_0$$

$$B(s) = s^3L^2C(1-k^2)k + sLk$$

$$C(s) = s^2Z_0LC(1-k^2) + sL + Z_0$$

$$D(s) = sLk$$

Therefore, the output I/Q magnitude and phase mismatches can be defined in equations (23) and (24).

$$I/Q\ \text{magnitude mismatch (dB)} = |20\log_{10}|S_{21}| - 20\log_{10}|S_{31}|| \tag{23}$$

$$I/Q\ \text{phase mismatch (°)} = \text{phase}(S_{21}) - \text{phase}(S_{31}) + 90° \tag{24}$$

Figure 4(a) and 4(b) show the simulated output I/Q magnitude and phase mismatches versus frequency of the high-k transformer 3 dB quadrature hybrid for different k values based on the equations (21)-(24). The design with k=0.707 and Z_0=50 **Ω** serves as the reference with the 3 dB quadrature hybrid operation at $\omega_{\lambda/4}=\omega_0=1$. The input matching ($S_{11}$) is shown in Fig. 4(c). The required inductances of the transformer-based 3 dB quadrature hybrid for different coupling k values are summarized in Fig. 3. The quarter-wave length frequency $\omega_{\lambda/4}$ for each coupling k is denoted in Fig. 4(c). Based on Fig. 4(a), although the transformer quadrature hybrid achieves equal power dividing only at one frequency point, a high-k design (k>0.707) provides one additional frequency point where excellent I/Q magnitude matching can be achieved. Within these two frequency points, a trade-off exists for the I/Q magnitude mismatch and matching bandwidth by adjusting the k value. Therefore, the I/Q matching bandwidth can be substantially extended. Note that a high-k design actually offers one more frequency point at high-frequency with good I/Q magnitude matching. However, this frequency point cannot be used in practice due to the substantial I/Q phase degradation. For example, the transformer design with k=0.75

achieves an I/Q 2 dB magnitude mismatch over a normalized bandwidth of 100% compared to a normalized bandwidth of 60% for the conventional design (k=0.707), shown in Fig. 4(a). In addition, the normalized bandwidth for I/Q phase mismatches below 5° increases from 126% for design with k=0.707 to 170% for design with k=0.75 (Fig. 4(b)). At the same time, the input matching bandwidth ($|S_{11}|$<-15 dB) extends from 130% to 174% after changing k from 0.707 to 0.75. These results demonstrate that a higher coupling coefficient k directly extends the bandwidth of the transformer quadrature hybrid. In practice, this high-k transformer quadrature hybrid design is limited by the achievable coupling coefficient k and the acceptable in-band I/Q magnitude mismatch. In this paper, we choose the coupling coefficient k=0.82 to achieve a compact transformer-based 3 dB quadrature hybrid at ω_0=6.8 Grad/s, and it is further utilized as a basic building block in our proposed transformer-based poly-phase network.

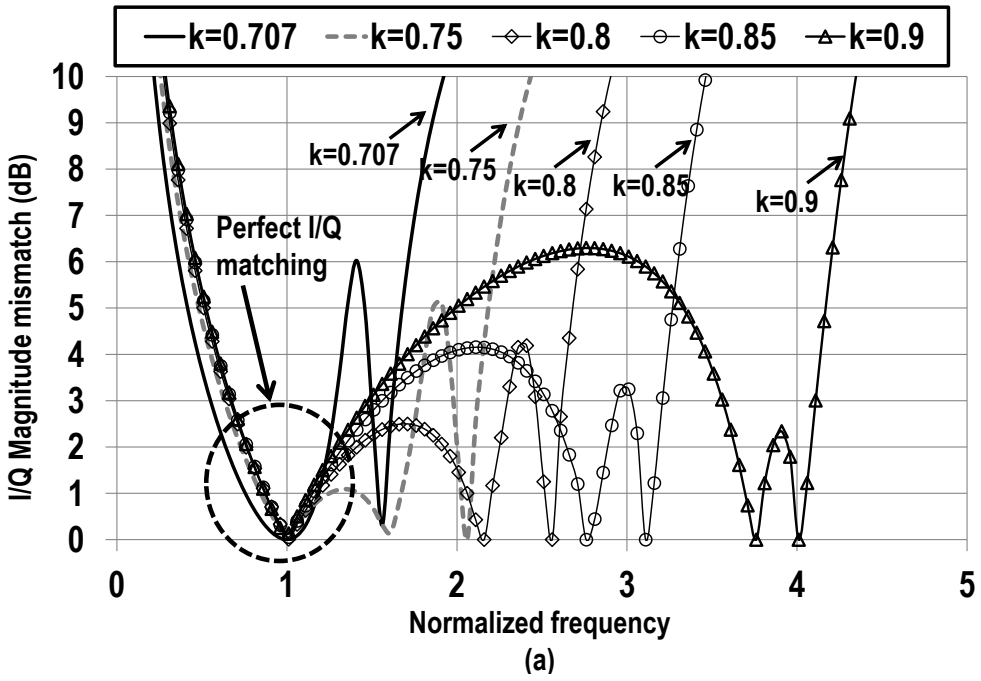

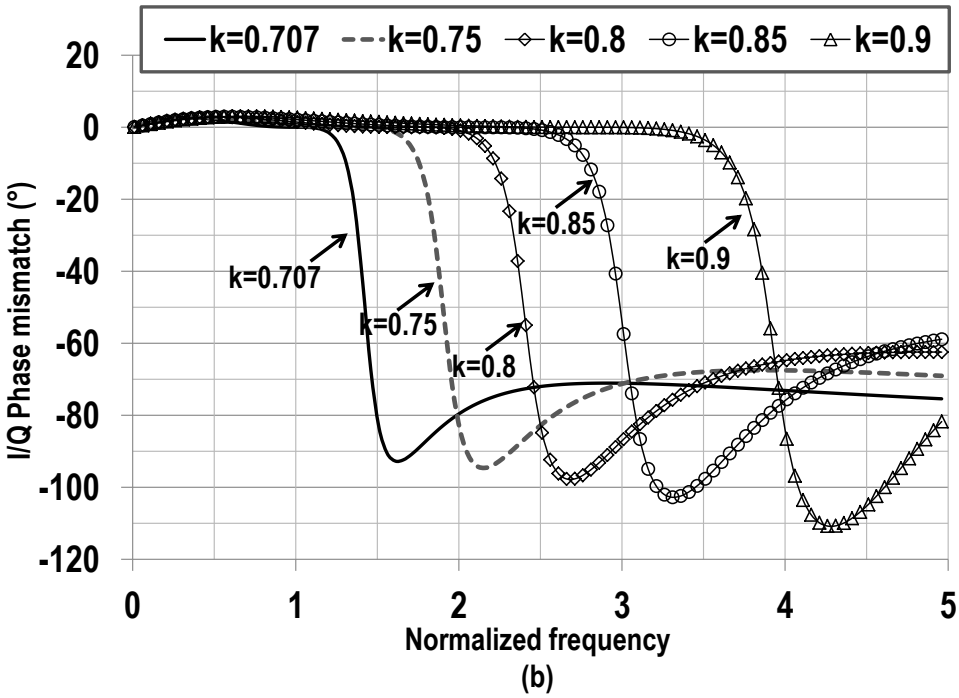

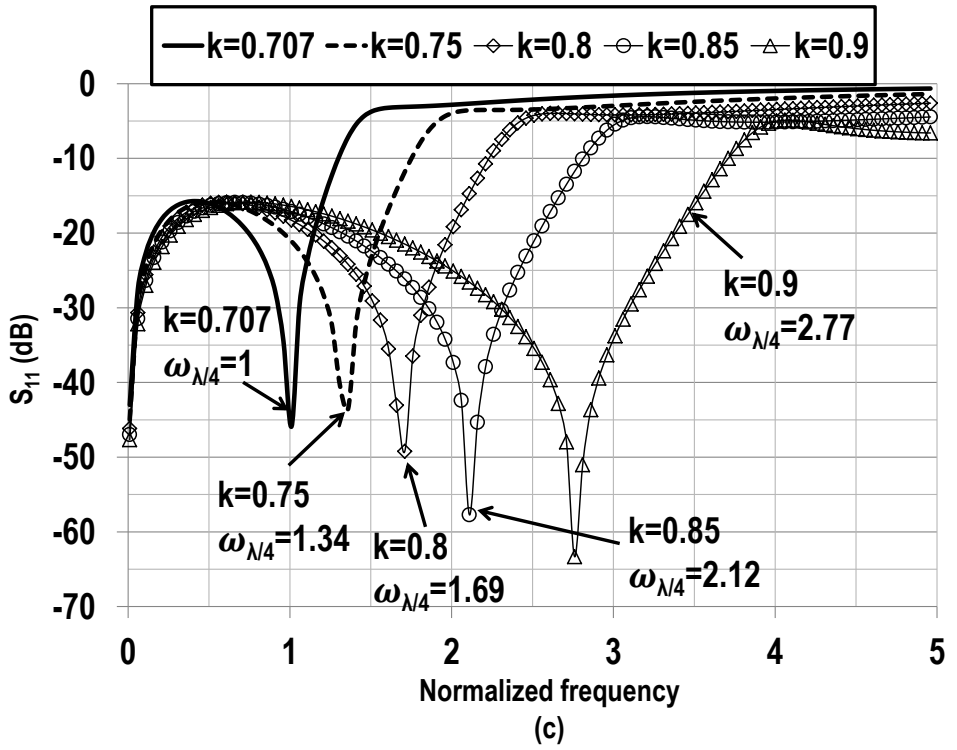

Fig. 4. The calculated (a) output I/Q magnitude mismatches, (b) I/Q phase mismatches, and (c) input matching S_{11} of the transformer-based 3 dB quadrature hybrids for different coupling k with ω_0=1. The calculations are based on the analytical equations (11)-(22).

CHAPTER III

TRANSFORMER-BASED POLY-PHASE NETWORK SCHEME

Although our proposed high-k transformer approach increases the bandwidth for the I/Q generation, it still exhibits trade-off with in-band I/Q magnitude mismatch, limiting the useful quadrature operation bandwidth in practice. In this section, we will introduce a multistage transformer-based poly-phase network scheme, which can suppress the I/Q magnitude/phase mismatches and achieve high-quality quadrature signals over an ultra-wide bandwidth. Different from conventional RC-CR poly-phase network, our transformer-based scheme has no resistive component in the signal paths. This aspect ensures its unique low-loss during multi-stage cascading.

A. Multistage Transformer-Based Poly-Phase Network

Figure 5 shows the block diagram of our proposed multistage transformer-based poly-phase network with N stages. It consists of one fully differential transformer-based quadrature hybrid as the 1st stage and N-1 stages of transformer-based poly-phase unit stage as the following cascaded stages. The 1st stage generates fully differential I/Q signals from a differential input. The cascaded N-1 transformer-based poly-phase unit stages then suppress the I/Q magnitude/phase mismatches from the 1st stage and substantially extend the I/Q generation bandwidth.

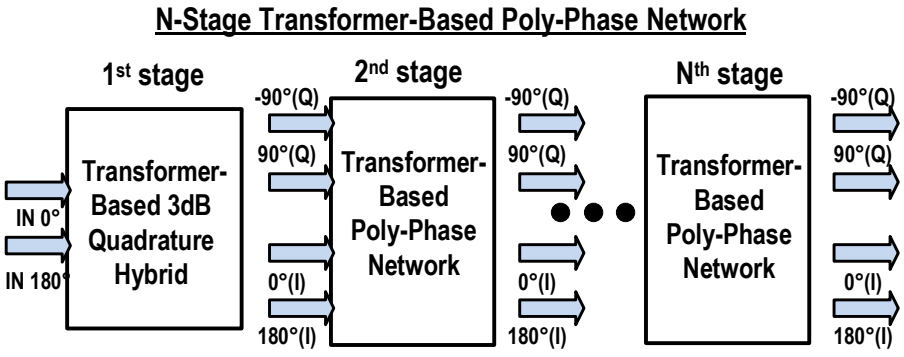

Fig. 5. The block diagram of the proposed multistage transformer-based poly-phase network with N stages.

B. A Transformer-Based Poly-Phase Unit Stage

The schematic of a transformer-based poly-phase unit stage is shown in Fig. 6. It consists of four single-ended transformer 3 dB quadrature hybrids and has 4 inputs and 4 outputs. Both inputs and outputs are 4 fully differential I/Q signals, making this poly-phase unit stage cascadable to realize the multistage poly-phase network configuration shown in Fig. 5.

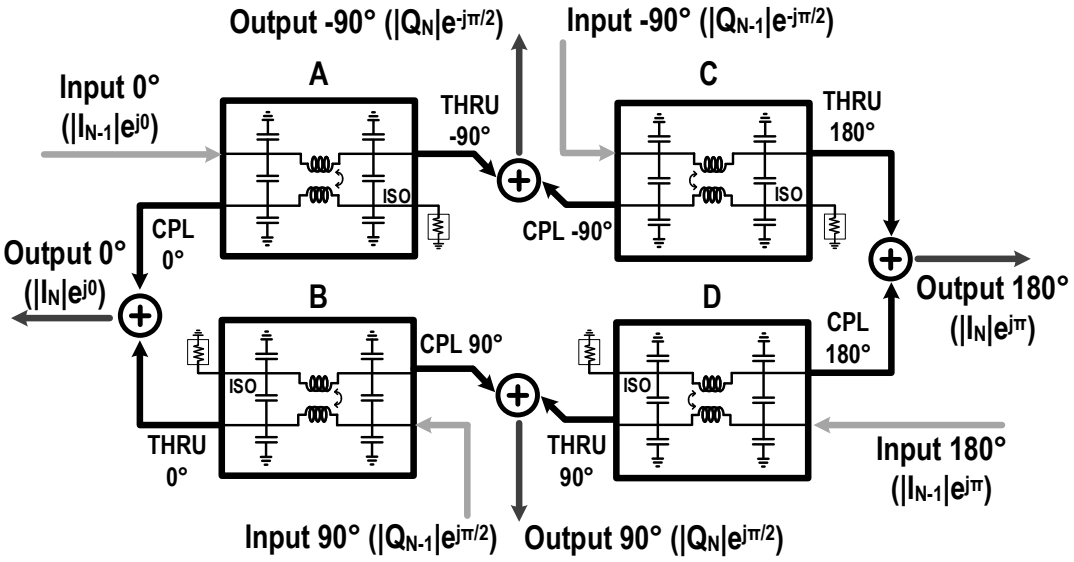

Fig. 6. Schematic of a transformer-based poly-phase unit stage.

The proposed transformer-based poly-phase unit stage in Fig. 6 employs four single-ended transformer 3 dB quadrature hybrids, which are arranged in such a way that the 4-output are generated by proper signal combining between the differential input I-signals ($|I_{N-1}|e^{j0}$ or $|I_{N-1}|e^{j\pi}$) and the differential input Q-signals ($|Q_{N-1}|e^{j\pi/2}$ or $|Q_{N-1}|e^{-j\pi/2}$). The four possible combinations (2×2) of the differential input I/Q signals result in the four outputs. For example, the output 0º (I+ or $|I_N|e^{j0}$) signal is generated by in-phase combining the input 0º ($|I_{N-1}|e^{j0}$) signal through the CPL-path of the transformer hybrid A with 0º phase shift and input 90º ($|Q_{N-1}|e^{j\pi/2}$) signal through the THRU-path of the transformer hybrid B with -90º phase shift. Therefore, when the input I/Q signals have magnitude/phase

mismatches, the transformer poly-phase unit stage will average out such mismatches. The operation principle of the poly-phase unit stage is demonstrated as follows by circuit analysis and analytical design equations.

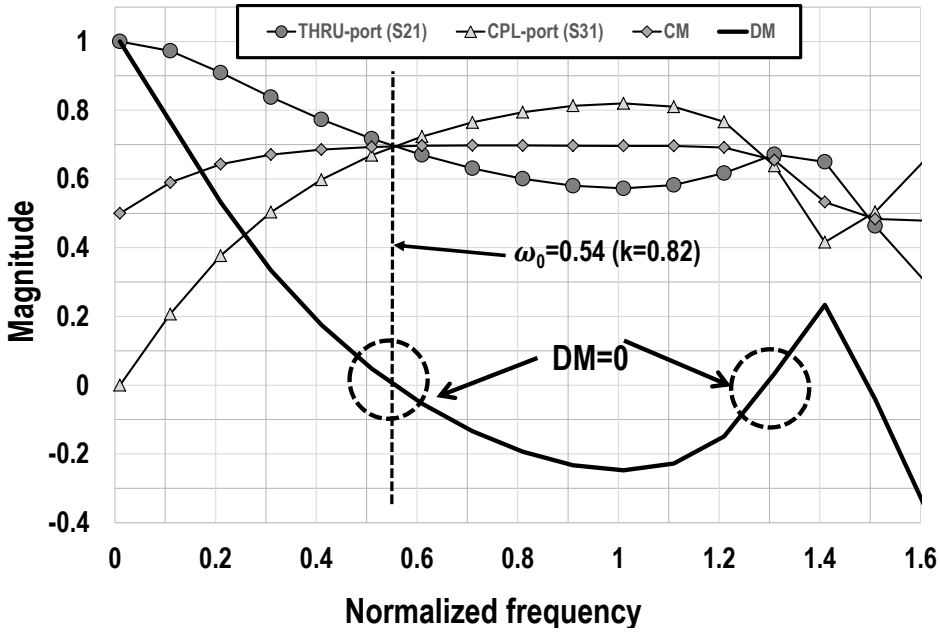

Fig. 7. The calculated magnitude response of the THRU-path (S_{21}) and CPL-path (S_{31}) together with their Common-Mode (CM) and Differential-Mode (DM) output signals based on (25) and (26). These results are based on a transformer quadrature hybrid with k=0.82, ω_0=0.54, and $\omega_{\lambda/4}$=1.

The magnitudes of the I (CPL-path) and Q (THRU-path) outputs of a transformer quadrature hybrid with k=0.82, ω_0=0.54, and $\omega_{\lambda/4}$=1 are shown in Fig. 7. The THRU-port (S_{21}) is lagging 90º behind the CPL-port and the normalized frequency ω_0 of the 3 dB quadrature hybrid operation is 0.54 (Fig. 2(a) and 2(b)). Note that the I/Q phase mismatch is below 10º from dc to a normalized frequency of 1.33 (Fig. 2(b)). Thus, we will focus on I/Q magnitude mismatch in the following discussions, since it is often the dominant mismatch compared with the I/Q phase mismatch in transformer quadrature hybrids.

Considering the CPL-path and THRU-path outputs (S_{31} and S_{21}), we can define the Common-Mode (CM) output and Differential-Mode (DM) output in equations (25)-(26) and plot them in Fig. 7. Note that the CM output has its magnitude variation of less than

0.15 dB from low-frequency (near dc) to a normalized frequency of 1.4 (Fig. 7), achieving an ultra-broadband flat frequency response. Within the frequency bandwidth where the I/Q 90° phase relationship holds, the complex I/Q outputs (S_{31} and S_{21}) can be represented by the CM and DM outputs in equations (27)-(28).

$$\mathrm{CM}(\omega) = \frac{1}{2}[|S_{21}(\omega)| + |S_{31}(\omega)|] \tag{25}$$

$$\mathrm{DM}(\omega) = \frac{1}{2}[|S_{21}(\omega)| - |S_{31}(\omega)|] \tag{26}$$

$$S_{21}(\omega) = [\mathrm{CM}(\omega) + \mathrm{DM}(\omega)]e^{-j\frac{\pi}{2}} \tag{27}$$

$$S_{31}(\omega) = [\mathrm{CM}(\omega) - \mathrm{DM}(\omega)]e^{j0} \tag{28}$$

Figure 8 summarizes the in-phase combining of the transformer-based poly-phase network at the Nth stage of the poly-phase unit stage. For the Nth unit stage, the differential I/Q outputs are derived and further expressed using CM and DM outputs in equations (29)-(32), within the frequency bandwidth where the I/Q 90° phase relationship holds.

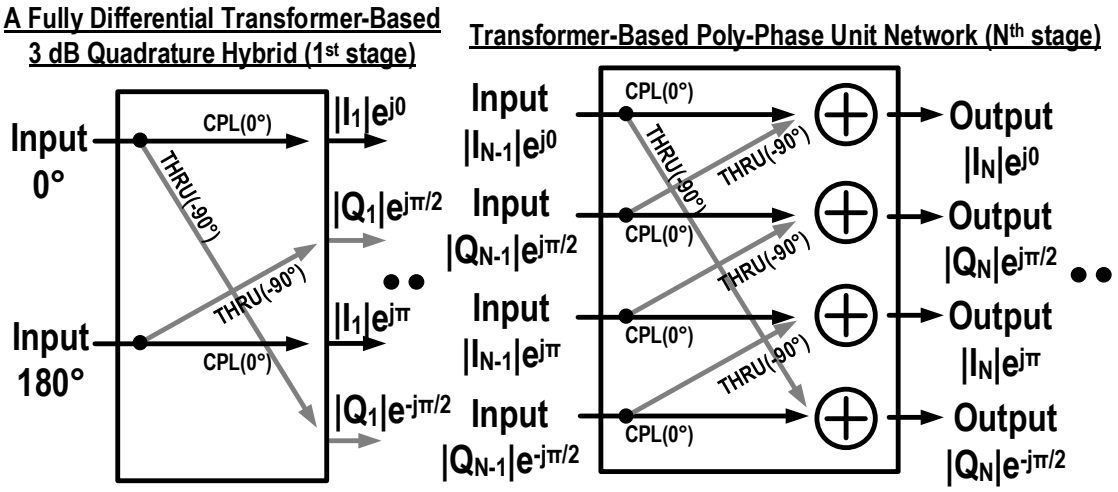

Fig. 8. Summary of the transformer-based poly-phase scheme.

$$|I_N|e^{j0}\ (\text{Output with } 0°) \tag{29}$$

$$= S_{21}(\omega) \times |Q_{N-1}|e^{\frac{j\pi}{2}} + S_{31}(\omega) \times |I_{N-1}|e^{j0}$$

$$= [(|I_{N-1}| + |Q_{N-1}|)CM(\omega) + (|Q_{N-1}| - |I_{N-1}|)DM(\omega)]e^{j0}$$

$$|Q_N|e^{\frac{-j\pi}{2}} \text{ (Output with } -90°) \quad (30)$$

$$= S_{21}(\omega) \times |I_{N-1}|e^{j0} + S_{31}(\omega) \times |Q_{N-1}|e^{\frac{-j\pi}{2}}$$

$$= [(|I_{N-1}| + |Q_{N-1}|)CM(\omega) + (|I_{N-1}| - |Q_{N-1}|)DM(\omega)]e^{\frac{-j\pi}{2}}$$

$$|I_N|e^{j\pi} \text{ (Output with } 180°) \quad (31)$$

$$= S_{21}(\omega) \times |Q_{N-1}|e^{\frac{-j\pi}{2}} + S_{31}(\omega) \times |I_{N-1}|e^{j\pi}$$

$$= [(|I_{N-1}| + |Q_{N-1}|)CM(\omega) + (|Q_{N-1}| - |I_{N-1}|)DM(\omega)]e^{j\pi}$$

$$|Q_N|e^{\frac{j\pi}{2}} \text{ (Output with } 90°) \quad (32)$$

$$= S_{21}(\omega) \times |I_{N-1}|e^{j\pi} + S_{31}(\omega) \times |Q_{N-1}|e^{\frac{j\pi}{2}}$$

$$= [(|I_{N-1}| + |Q_{N-1}|)CM(\omega) + (|I_{N-1}| - |Q_{N-1}|)DM(\omega)]e^{\frac{j\pi}{2}}$$

$|I_{N-1}|$ and $|Q_{N-1}|$ denote the input I and Q magnitudes, while the output I and Q magnitudes are represented by $|I_N|$ and $|Q_N|$. Therefore, based on equations (29)-(32), the output I/Q magnitude mismatches of the N^{th} stage output are given as

$$\big||I_N| - |Q_N|\big| = 2\big(\big||I_{N-1}| - |Q_{N-1}|\big|\big)|DM(\omega)|. \quad (33)$$

C. The Cascaded Multistage Poly-Phase Network Behavior

Next, we will investigate the cascaded multistage transformer-based poly-phase network behavior, in particular the suppression on the I/Q magnitude and phase mismatches. Based on (33), by passing the I/Q signals through a transformer poly-phase unit stage, the I/Q magnitude mismatches can be suppressed within the frequency range where $|DM(\omega)| \leq 1/2$ holds for the unit stage. For an N-stage transformer-based poly-phase network, the resulting I/Q magnitude mismatch at the network output can be expressed in equation (34)

$$||I_N| - |Q_N|| = ||I_1| - |Q_1|| \times [|2DM(\omega)|]^{N-1}, \quad (34)$$

where $||I_1| - |Q_1||$ represents the I/Q magnitude mismatch due to the 1st stage transformer quadrature hybrid stage and $[|2DM(\omega)|]^{N-1}$ is the mismatch suppression effect by the following N-1 stages of transformer poly-phase unit stages. If the 1st stage and the following N-1 unit stages adopt the same differential transformer-based quadrature hybrid design, they present the same Differential-Mode output component DM(ω). Thus, the total output I/Q magnitude mismatch of the N-stage transformer poly-phase network is thus given by equation (35).

$$||I_N| - |Q_N|| = 2|DM(\omega)| \times [2|DM(\omega)|]^{N-1} = [2|DM(\omega)|]^N \quad (35)$$

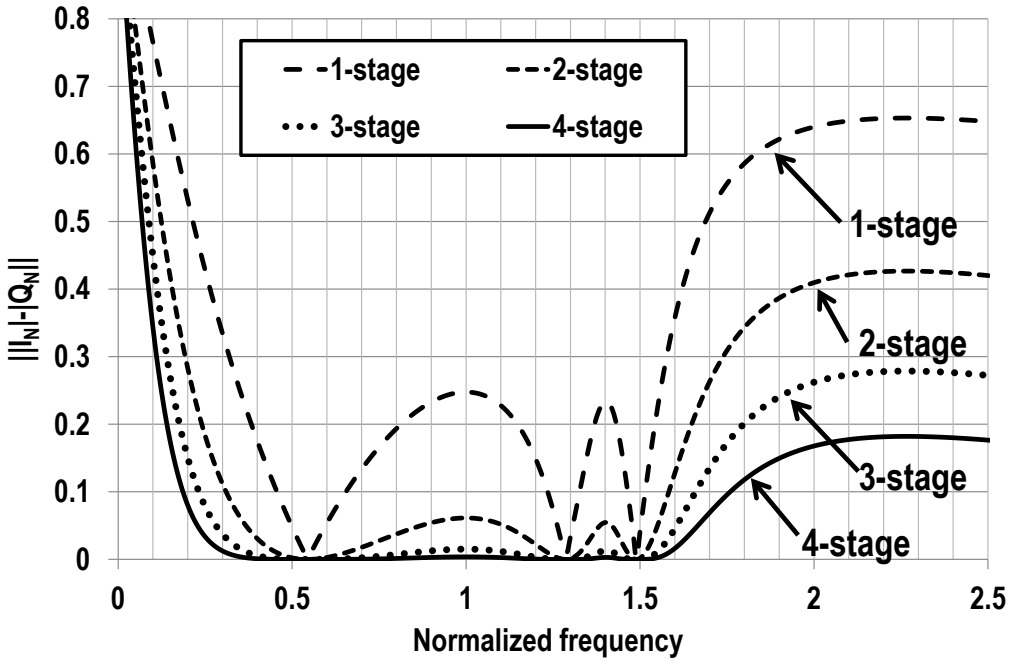

Fig. 9. The calculated I/Q magnitude mismatch suppression versus the number of stages of the multistage transformer-based poly-phase network based on equation (26) and (35).

Figure 9 summarizes the calculated I/Q magnitude mismatch versus the number of stages of the transformer poly-phase network based on equations (26) and (35) for a transformer quadrature hybrid design with k=0.82, ω_0=0.54<$\omega_{\lambda/4}$=1, and Z_0=50 Ω. The I/Q magnitude mismatch is largely suppressed as the number of stages increases in Fig. 9.

Next, we will investigate the I/Q phase mismatches suppression by the proposed multistage transformer-based poly-phase network. We assume that the unit poly-phase stage (Fig. 6) is composed of four identical phase-mismatched transformer-based 3 dB quadrature hybrids. An effective phase error θ is added at the THRU-path of each hybrid output (270°), while the CPL-path phase response remains as 0º, shown in equations (36)-(37). This effective phase error θ captures the phase errors due to electromagnetic simulation inaccuracy and device modelling errors in practice.

$$S_{21}(\omega) = [CM(\omega) + DM(\omega)]e^{-j\frac{\pi}{2}}e^{j\theta} \tag{36}$$

$$S_{31}(\omega) = [CM(\omega) - DM(\omega)]e^{j0} \tag{37}$$

For the input I/Q phase errors of the N^{th}-stage transformer-based poly-phase unit stage in Fig. 6, we add phase error term (θ_{N-1}) at the differential input Q signals. Therefore, the input differential I/Q signals are denoted as $|I_{N-1}|e^{j0}$, $|I_{N-1}|e^{j\pi}$, $|Q_{N-1}|e^{j\pi/2}e^{j(\theta N-1)}$, and $|Q_{N-1}|e^{-j\pi/2}e^{j(\theta N-1)}$ for the N^{th}-stage unit stage. Based on the proposed N-stage transformer-based poly-phase network shown in Fig. 5 and Fig. 8, the differential input I/Q signals of the 2^{nd}-stage poly-phase network are generated from the 1^{st}-stage differential transformer 3 dB quadrature hybrid. Specifically, the differential I outputs ($|I_1|e^{j0}$ and $|I_1|e^{j\pi}$) are generated through the two CPL-paths and the differential Q outputs ($|Q_1|e^{j\pi/2}$ and $|Q_1|e^{-j\pi/2}$) are generated from the two THRU-paths in the 1^{st} stage hybrid shown in Fig. 8. Therefore, if identical transformer quadrature hybrids are used in the 1^{st} stage and the following N-1 unit stages, θ_1 thus equals θ. The output I/Q phase error at the N^{th}-stage transformer-based poly-phase unit stage outputs (θ_N) are derived below in equations (38)-(44).

$$\text{Complex Output I } (0°) \tag{38}$$

$$= S_{21}(\omega) \times |Q_{N-1}|e^{j\frac{\pi}{2}}e^{j\theta_{N-1}} + S_{31}(\omega) \times |I_{N-1}|e^{j0}$$

$$= \left[|S_{21}(\omega)||Q_{N-1}|e^{j(\theta+\theta_{N-1})} + |S_{31}(\omega)||I_{N-1}|e^{j0}\right]e^{j0}$$

$$\text{mag(Output I)} \tag{39}$$

$$= \sqrt{\begin{matrix}(|S_{21}(\omega)||Q_{N-1}|)^2 + (|S_{31}(\omega)||I_{N-1}|)^2 \\ +2|S_{21}(\omega)||Q_{N-1}||S_{31}(\omega)||I_{N-1}|\cos(\theta+\theta_{N-1})\end{matrix}}$$

$$\text{phase(Output I)} \tag{40}$$

$$= \tan^{-1}\frac{|S_{21}(\omega)||Q_{N-1}|\sin(\theta+\theta_{N-1})}{|S_{31}(\omega)||I_{N-1}| + |S_{21}(\omega)||Q_{N-1}|\cos(\theta+\theta_{N-1})}$$

$$+0°$$

$$\text{Complex Output Q } (-90°) \tag{41}$$

$$= S_{21}(\omega) \times |I_{N-1}|e^{j0} + S_{31}(\omega) \times |Q_{N-1}|e^{-\frac{j\pi}{2}}e^{j\theta_{N-1}}$$

$$= \left[|S_{21}(\omega)||I_{N-1}|e^{j(\theta-\theta_{N-1})} + |S_{31}(\omega)||Q_{N-1}|\right]e^{\frac{-j\pi}{2}}e^{j\theta_{N-1}}$$

$$\text{mag(Output Q)} \tag{42}$$

$$= \sqrt{\begin{matrix}(|S_{21}(\omega)||I_{N-1}|)^2 + (|S_{31}(\omega)||Q_{N-1}|)^2 \\ +2|S_{21}(\omega)||I_{N-1}||S_{31}(\omega)||Q_{N-1}|\cos(\theta-\theta_{N-1})\end{matrix}}$$

$$\text{phase(Output Q)} \tag{43}$$

$$= \tan^{-1}\frac{|S_{21}(\omega)||I_{N-1}|\sin(\theta-\theta_{N-1})}{|S_{31}(\omega)||Q_{N-1}| + |S_{21}(\omega)||I_{N-1}|\cos(\theta-\theta_{N-1})}$$

$$-90° + \theta_{N-1}$$

$$\text{output I/Q phase mismatch } (\theta_N) \tag{44}$$

$$= \tan^{-1}\frac{|S_{21}(\omega)||Q_{N-1}|\sin(\theta+\theta_{N-1})}{|S_{31}(\omega)||I_{N-1}| + |S_{21}(\omega)||Q_{N-1}|\cos(\theta+\theta_{N-1})}$$

$$-\tan^{-1}\frac{|S_{21}(\omega)||I_{N-1}|\sin(\theta-\theta_{N-1})}{|S_{31}(\omega)||Q_{N-1}| + |S_{21}(\omega)||I_{N-1}|\cos(\theta-\theta_{N-1})}$$

$$-\theta_{N-1}$$

It is of particular interest to investigate the I/Q phase mismatch suppression at the normalized frequency above 1, where I/Q phase mismatch becomes more significant (Fig. 2). The magnitude of |DM(ω)| defined in (26) is small at the normalized frequency above 1 and DM(ω)=0 at ω=1.33. Therefore, $|S_{31}(\omega)| \cong |S_{21}(\omega)|$. Furthermore, as the number of stages of the transformer poly-phase network increases, I/Q magnitude mismatches ($||I_{N-1}|$-

$|Q_{N-1}|$) are suppressed based on equations (34)-(35), and then $|I_{N-1}| \cong |Q_{N-1}|$ in Fig. 9. Therefore, $|S_{31}(\omega)| \times |Q_{N-1}| \cong |S_{21}(\omega)| \times |I_{N-1}|$ and $|S_{31}(\omega)| \times |I_{N-1}| \cong |S_{21}(\omega)| \times |Q_{N-1}|$ at the normalized frequency above 1. Therefore, the equation (44) can be further expressed as

$$\text{output I/Q phase mismatch } (\theta_N) \cong \tag{45}$$

$$\tan^{-1}\frac{\sin(\theta+\theta_{N-1})}{1+\cos(\theta+\theta_{N-1})} - \tan^{-1}\frac{\sin(\theta-\theta_{N-1})}{1+\cos(\theta-\theta_{N-1})} - \theta_{N-1}$$

$$= \frac{(\theta+\theta_{N-1})}{2} - \frac{(\theta-\theta_{N-1})}{2} - \theta_{N-1} = 0.$$

The equation (45) shows that the quadrature phase mismatch due to the phase error θ of the transformer quadrature hybrid is also largely suppressed by the N-stage poly-phase network, as a result of the quadrature amplitude mismatch suppression. This directly reduced the output I/Q phase mismatches and extends the quadrature operation bandwidth.

In summary, the proposed transformer-based poly-phase network suppresses both magnitude and phase mismatches of the I/Q signals and achieves an ultra-broadband operation.

CHAPTER IV

A TRANSFORMER-BASED POLY-PHASE NETWORK DESIGN EXAMPLE

In this section, we will present a proof-of-concept 3-stage transformer-based poly-phase network design ($\omega_0 = 2\pi \times 6.8$ Grad/s) with its design process and simulation results to demonstrate the proposed concept. The 3-stage transformer-based poly-phase network system architecture is shown in Fig. 10. A fully differential 8-port folded transformer quadrature hybrid serves as the 1st stage to generate the differential I/Q signals [12]. The same hybrid design is also employed in the transformer poly-phase unit stage, which is composed of two identical hybrid designs to process and generate differential quadrature signals. Two poly-phase unit stages are cascaded after the 1st stage to form the 3-stage poly-phase network.

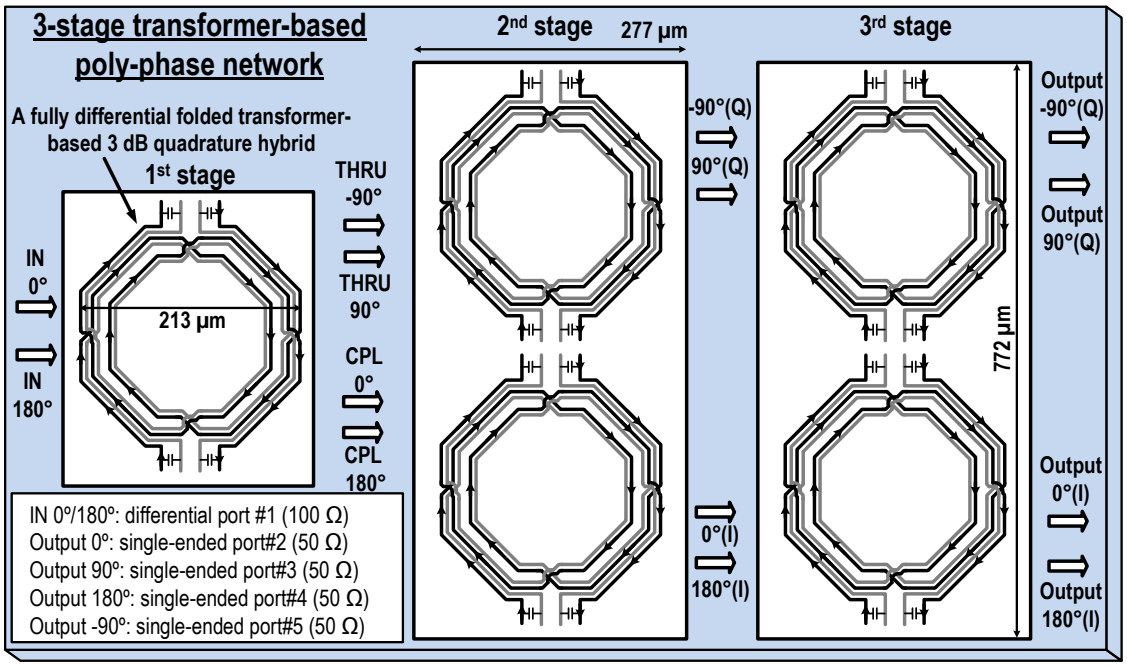

Fig. 10. The implementation of the 3-stage transformer-based poly-phase network ($\omega_0 = 2\pi \times 6.8$ Grad/s).

The design of the fully differential 8-port folded transformer 3 dB quadrature hybrid [12] with $\omega_0=2\pi\times6.8$ Grad/s is explained as follows (Fig. 11). Two single-ended transformer quadrature hybrids (TRF1 and TRF2) are first implemented by following the design equations in Section II, and the hybrid structure is modeled using 3D EM simulations. The differential operation allows folding these two single-ended transformer quadrature hybrids (TRF1 and TRF2) into only one-inductor foot print. The two separate single-ended transformer-based quadrature hybrids (TRF1 and TRF2) are first arranged as shown in Fig. 11 to ensure identical current flow directions, when being excited by differential signals. Therefore, folding TRF1 and TRF2 together can be achieved for significant size reduction. Moreover, this folded transformer exploits the positive magnetic coupling of $k_f=0.36$ between the two single-ended transformer hybrids (TRF1 and TRF2), resulting in a larger effective inductance ($L_{eff}=L+k_fL$). Such magnetic enhancement allows the further size reduction as well as low loss operation at the desired differential mode. Note that this magnetic coupling k_f is simply the result of folding two transformer hybrids together, and it is different from the magnetic coupling k in designing the transformer quadrature hybrid itself in Section II.

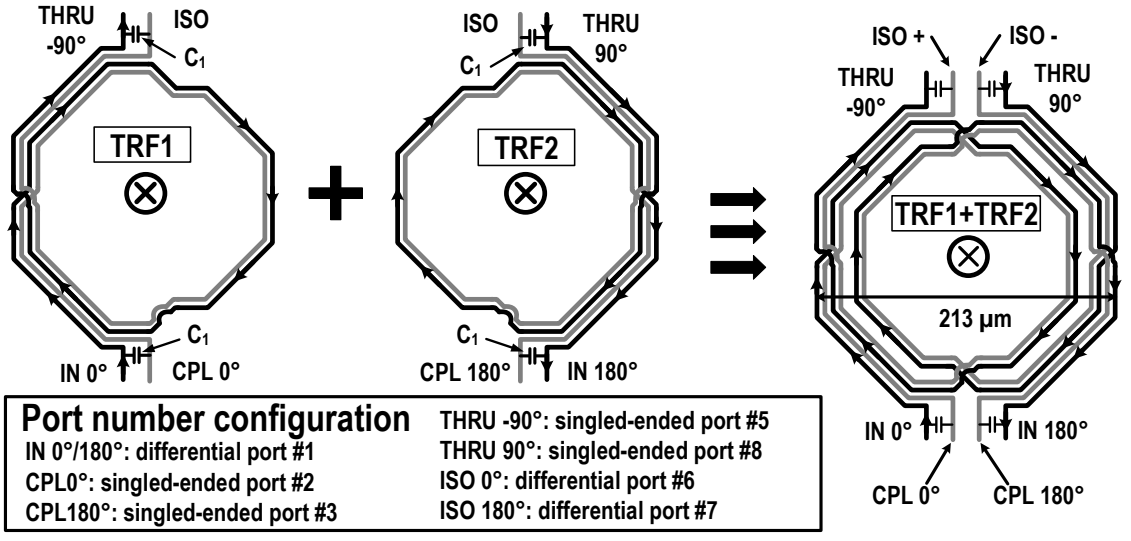

Fig. 11. The 8-port folded transformer quadrature hybrid to generate a fully differential I/Q signals within one inductor footprint.

The parasitic ground capacitances of the physical transformer can be absorbed in the C_G in Fig. 1 and the parasitic inter-winding capacitance can be absorbed in the C_M in Fig. 1. Extra Metal-Oxide-Metal (MOM) capacitors (C_1) are added to achieve the desired the capacitive coupling C_M in Fig. 11. Figure 12 shows the simulated I/Q magnitude and phase of the differential folded transformer quadrature hybrid. The coupling coefficient k of each transformer hybrid is 0.82 at 6.8 GHz. The input is driven differentially by a differential 100 Ω input port (port1) and the other 6-ports are each terminated with a single-ended 50 Ω load. Since the differential input power is equally dividing into four single-ended ports, the fundamental power dividing loss is 6 dB. The simulated passive loss due to the transformer quadrature hybrid structure is thus 0.4 dB (Fig. 12(a)). The I/Q magnitude mismatch is less than 1 dB from 5.8 GHz to 7.6 GHz, and the I/Q phase mismatch is less than 5° from 0.1 GHz to 19 GHz for this one-stage differential transformer quadrature hybrid. The input matching S_{11} is below-10 dB from 0.1 GHz to 28 GHz, and the isolation is below -20 dB from 0.1 GHz to 26 GHz. The corresponding port definitions are shown in Fig. 11.

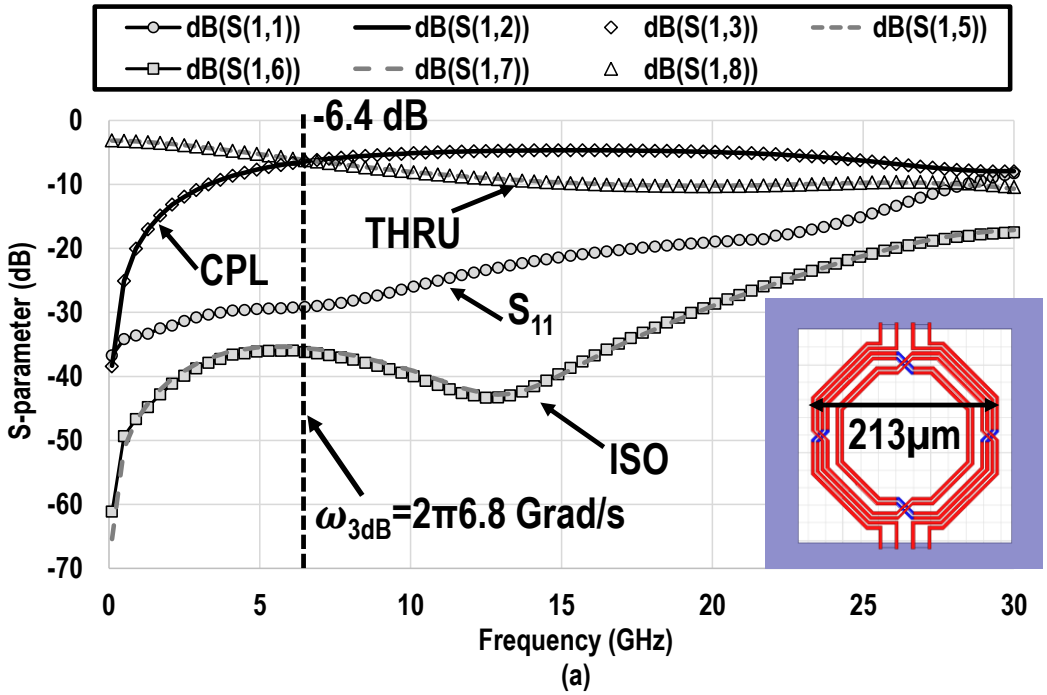

(a)

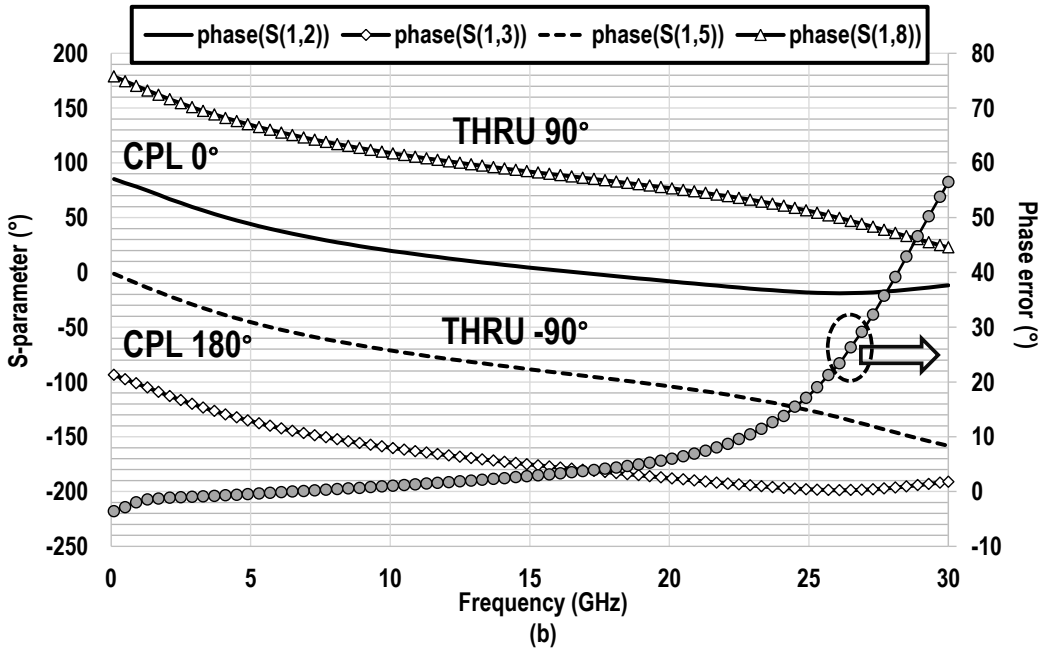

Fig. 12. The simulated (a) magnitude and (b) phase responses of the differential 8-port folded transformer quadrature hybrid based on full 3D EM modelling. The port definitions are shown in Fig. 11.

Based on Fig. 6, a direct implementation of the transformer poly-phase unit stage requires four single-ended transformer 3 dB quadrature hybrids. Since the inputs and the outputs of the coupler A/B and the coupler D/C have differential relationship (Fig. 6), thus two folded differential transformer quadrature hybrids can equivalently replace four single-ended quadrature hybrids to achieve a substantial size reduction. Figure 13 demonstrates the transformer-based poly-phase unit stage (Fig. 6) based on combining two differential 8-port folded transformer quadrature hybrids. Differential 100 Ω micro-strip transmission lines are added for signal routing and parallel in-phase power combining. Due to the parallel combining at the 4 outputs, their impedance values are differential 50 Ω, i.e., single-ended 25 Ω, resulting in a non-perfect but acceptable output matching of -9.5 dB. The reflected signals at the 4 outputs are absorbed by the termination resistors at the isolation ports of the transformer hybrids without affecting the input matching. The total simulated passive loss of this poly-phase unit stage is 0.6 dB based on 3D EM modeling.

The additional meander lines for phase-matched signal routing are not shown for simplicity.

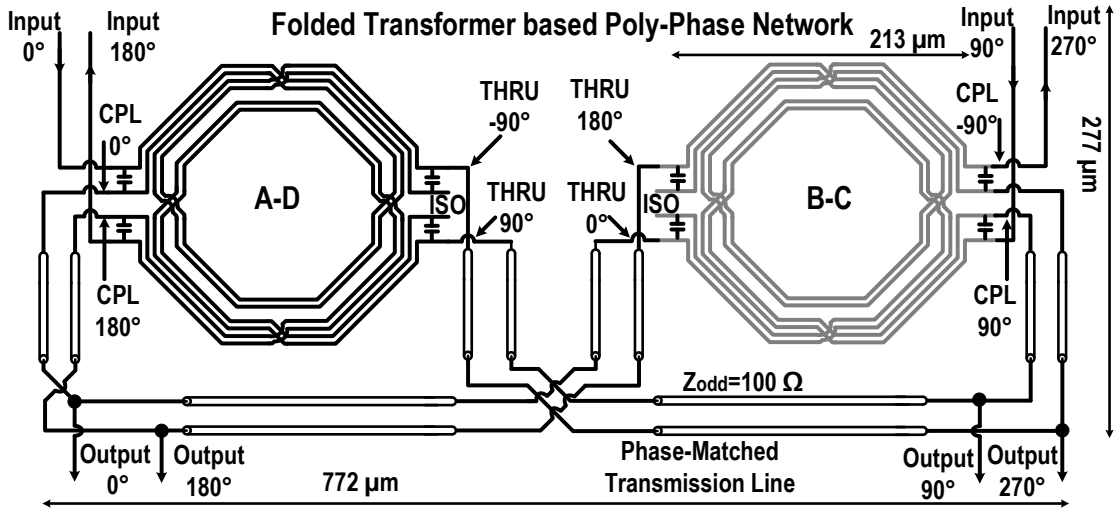

Fig. 13. A transformer poly-phase unit stage implemented using two 8-port folded transformer 3 dB quadrature hybrids. The meander lines for phase-matched routing are not shown for simplicity. The equivalent schematic is shown in Fig. 6.

Finally, we implement a 3-stage transformer poly-phase network (Fig. 5) with its 3D EM model shown in Fig. 14(a). The magnitude and phase responses are simulated based on the 3D EM modelling and shown in Fig. 14(b) and Fig. 14(c), respectively. The input (port1) is driven differentially by a differential 100 Ω port and the 4 outputs (port2-port5) are each terminated with a single-ended 50 Ω port (Fig. 14(a)), and the theoretical loss of the poly-phase network is 6 dB due to the 1:4 power dividing. Based on 3D EM modeling, the simulated passive loss is only 3.1 dB for the 3-stage transformer-based poly-phase network at 6.8 GHz (Fig. 14(b)). The simulated I/Q magnitude mismatch is lower than 1 dB from 2.9 GHz to 27 GHz, and the I/Q phase mismatch has its maximum value of 5º at 26 GHz. The input matching (S_{11}) is below -10 dB from 0.7 GHz to 24.5 GHz.

The I/Q magnitude and phase mismatches at the outputs of the 1st stage and the 2nd stage are also simulated based on the full 3D EM models and plotted in Fig. 15. The simulated I/Q magnitude mismatch is below 1 dB from 5.8 GHz to 7.6 GHz at the 1st stage

output (including the input signal pads and signal distribution lines). The simulated 1 dB I/Q magnitude mismatch at the 2nd stage output is satisfied from 4 GHz to 12.5 GHz and 20 GHz to 27 GHz. At the output of the 3rd stage, the simulated 1 dB I/Q mismatch bandwidth is from 2.9 GHz to 27 GHz. It is clear that cascading more transformer poly-phase stages directly suppresses the I/Q magnitude mismatch and extend the I/Q generation bandwidth. Note that the I/Q magnitude mismatch below 2.9 GHz cannot be efficiently suppressed, since the I/Q magnitude mismatch suppression condition, i.e., $|DM(\omega)|\leq 1/2$, cannot be satisfied in this low frequency range. This also aligns well with our theoretical derivations (Section III). The simulated I/Q phase mismatch is within 5º from 0.1 GHz to 12.5 GHz at the 1st stage output and from 0.1 GHz to 24 GHz for the 2nd stage output. This 5º I/Q phase mismatch bandwidth is further extended to 0.1 GHz to 26 GHz at the 3rd stage output. Therefore, cascading more transformer poly-phase stages also suppresses the I/Q phase mismatch and extend the I/Q generation bandwidth. In summary, these simulation results verify that our proposed multi-stage transformer-based poly-phase network achieves high-quality low-loss differential quadrature signal generation over an ultra-wide (one-decade) bandwidth.

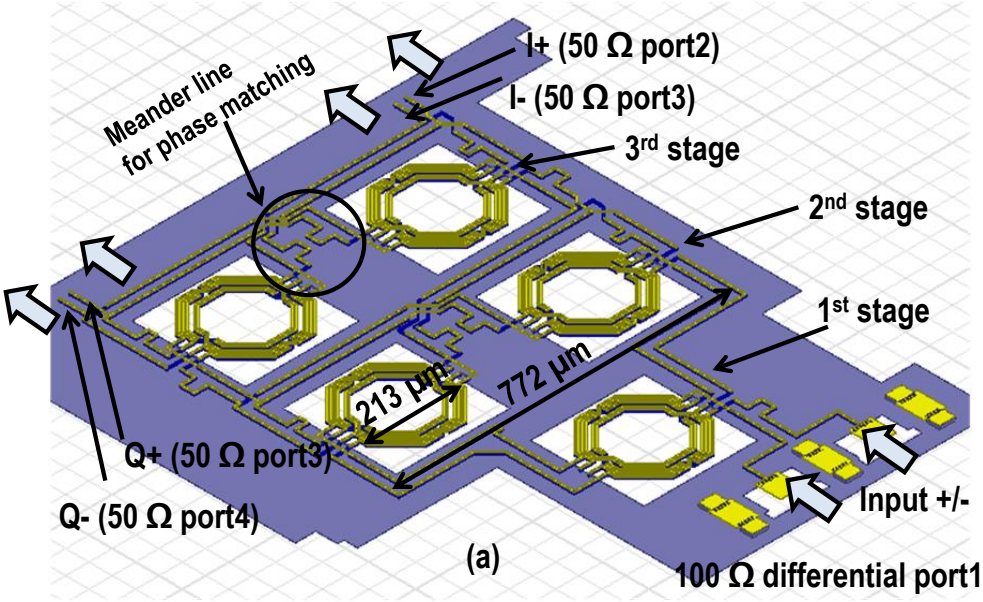

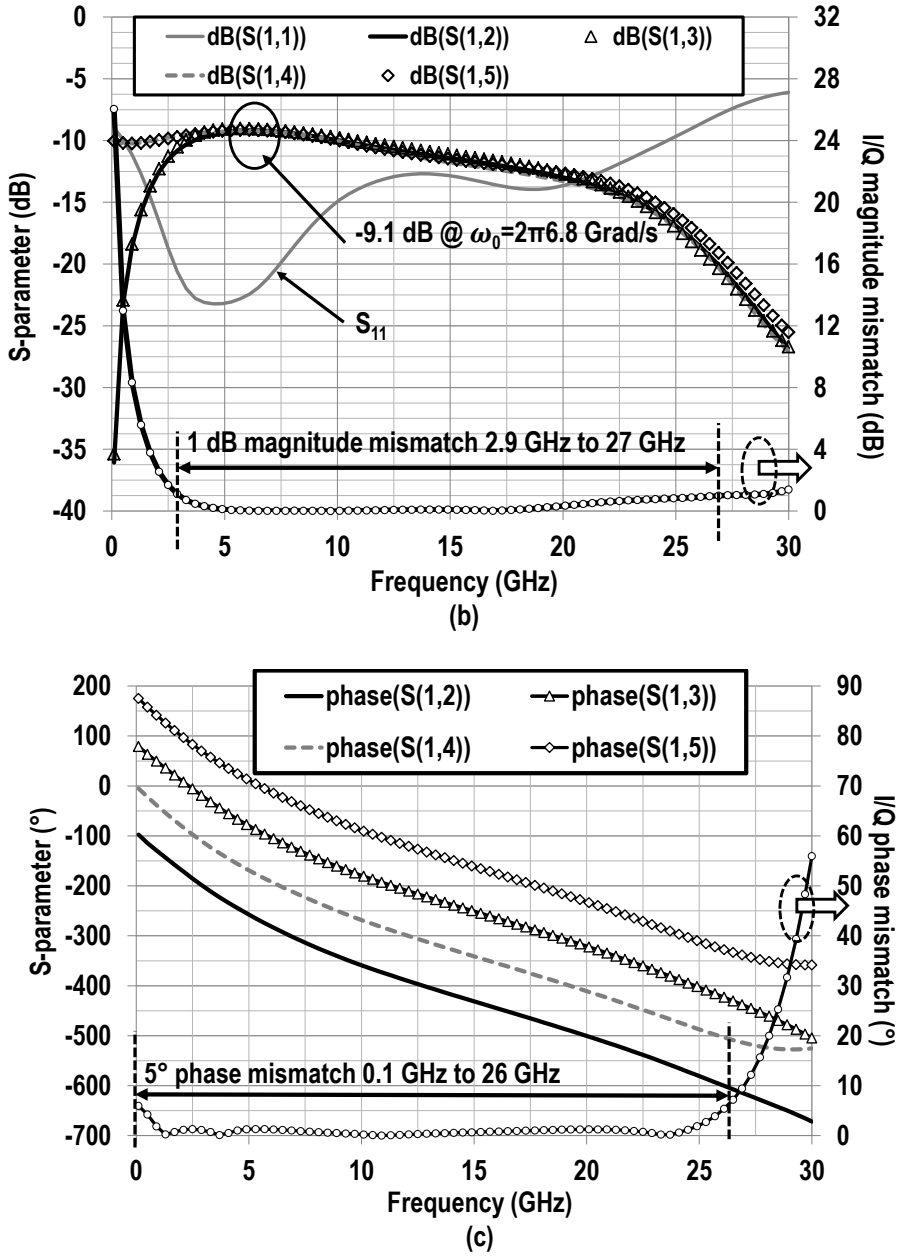

Fig. 14. (a) Full 3D EM model of the proposed 3-stage transformer-based poly-phase network. (b) Simulated magnitude and (c) phase responses of the proposed 3-stage transformer-based poly-phase network based on full 3D EM modelling. The port numbers are defined in Fig. 14(a).

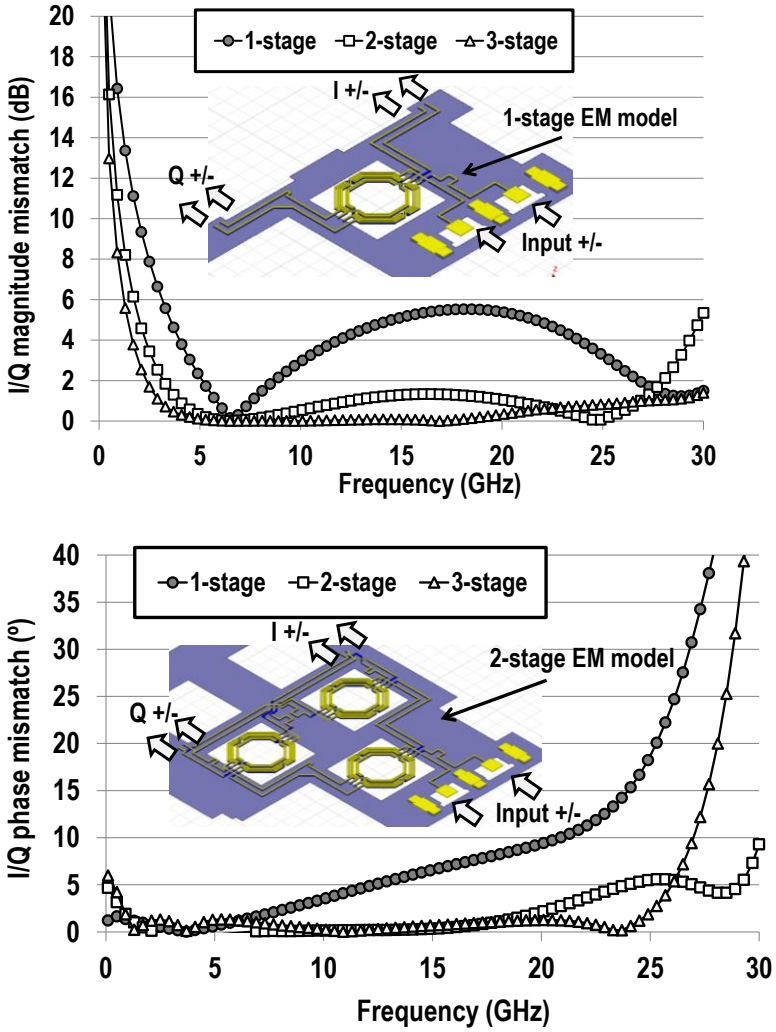

Fig. 15. Simulated output magnitude and phase mismatches for each stage in the example 3-stage transformer poly-phase network.

The EM simulated insertion loss is approximately 1 dB/stage. This is mainly due to the finite quality factor of the transformers (0.4 dB), the phase-matched transmission line loss for a signal routing (0.2 dB), and non-perfect output matching (0.4 dB). The insertion loss increases at the high frequency due to the quality factor degradation (skin effect) at the high frequency. However, this insertion loss result including the routing parasitic is much lower than a typical RC-CR based poly-phase network, since this transformer-based poly-phase network does not require any explicit resistive components in the RF signal paths.

CHAPTER V

MEASUREMENT RESULTS

The proof-of-concept 3-stage transformer-based poly-phase network design is implemented in a standard 65 nm bulk CMOS process with a low resistivity substrate ρ_{sub}=0.5 Ω·cm (Fig. 16) [16]. A differential 8-port folded transformer quadrature hybrid (k=0.82 and outer diameter=213 μm) serves as the 1st stage network. The same quadrature hybrid is also utilized to realize the two transformer poly-phase unit stages, and each unit stage occupies 277 μm×772 μm including the signal routings (Fig. 16). The core chip area of the 3-stage transformer-based poly-phase network is only 772 μm×925 μm, demonstrating a very compact foot print.

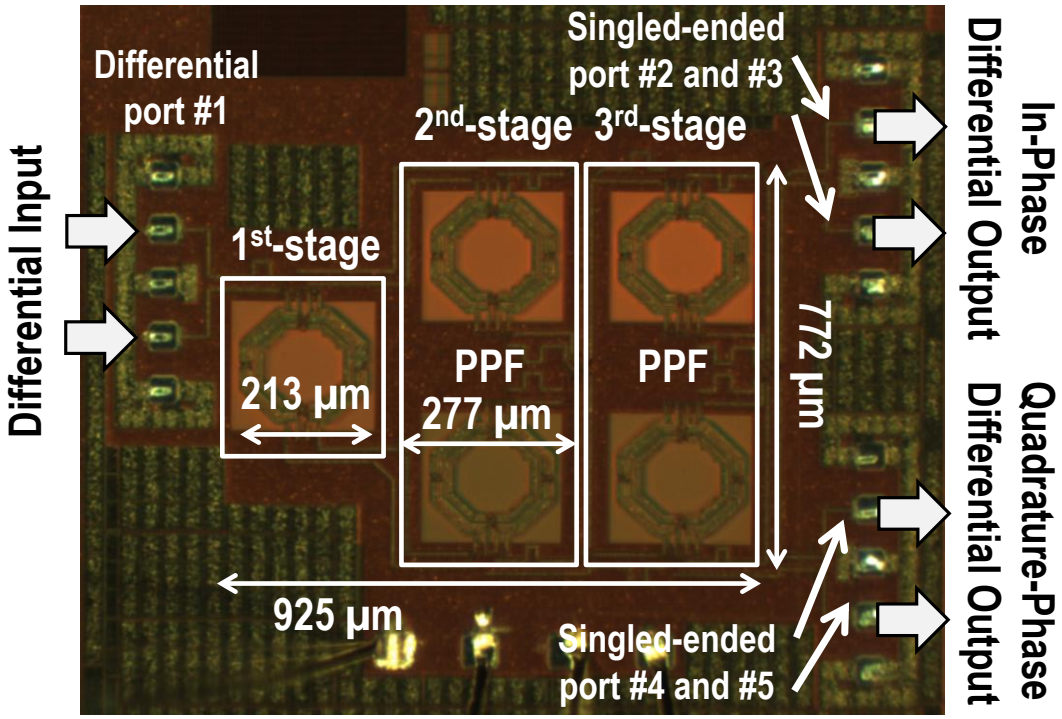

Fig. 16. The chip microphotograph of the proof-of-concept 3-stage transformer-based poly-phase network design.

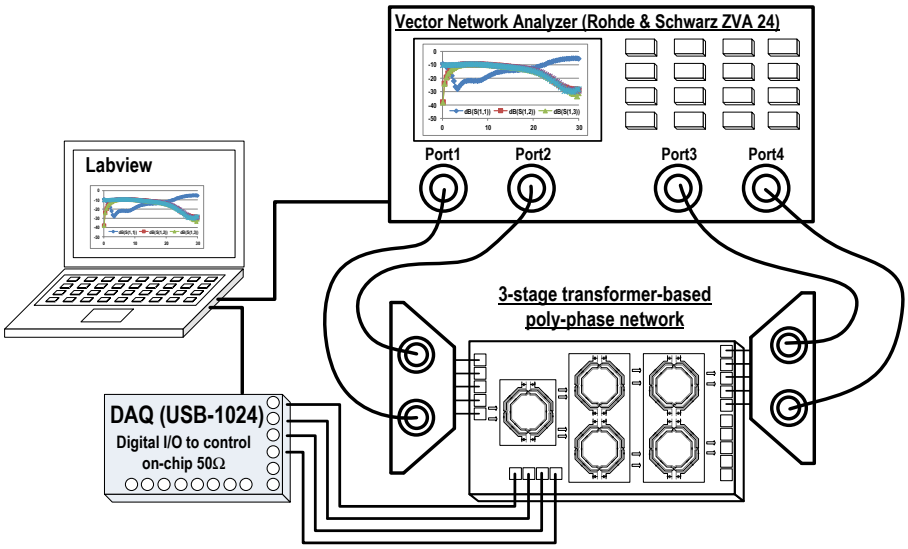

Fig. 17. Measurement setup to characterize the 3-stage transformer poly-phase network.

Since the passive network has one differential input (differential port 1) and two differential outputs (ports 2 to 5), on-chip 50 Ω terminations are implemented at all the ports and controlled by a digital code to facilitate the testing. By selectively terminating the unused ports with high-precision 50 Ω on-chip termination resistors, the 6-port 3-stage transformer poly-phase network thereby can be characterized by a 4-port vector network analyzer (Rohde & Schwarz ZVA 24). Three independent CMOS chip samples are measured, and the measurement results are summarized in Fig. 18.

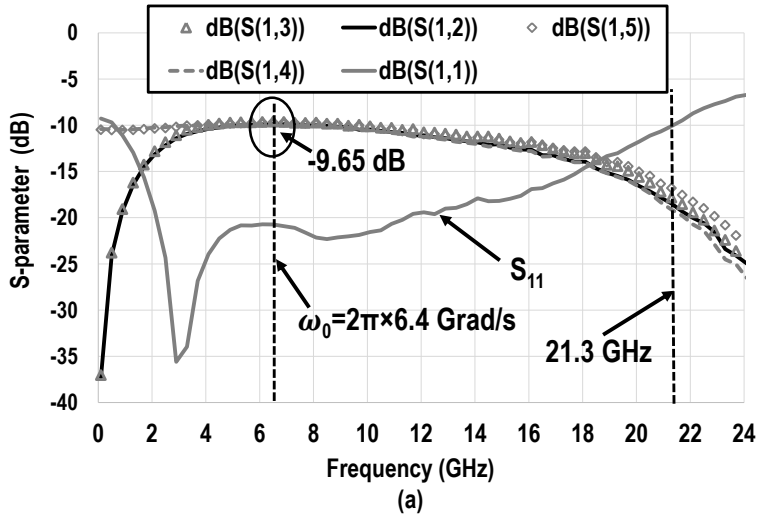

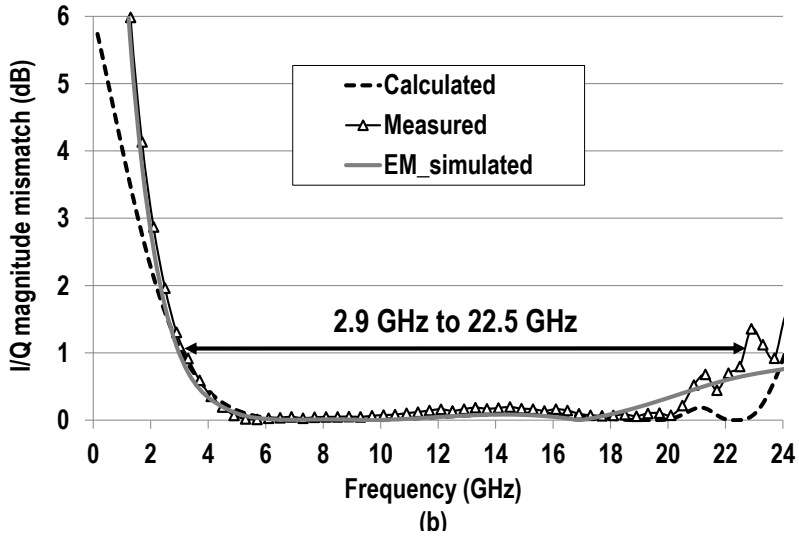
I/Q magnitude mismatch (dB)
Calculated
Measured
EM_simulated
2.9 GHz to 22.5 GHz
Frequency (GHz)

(b)

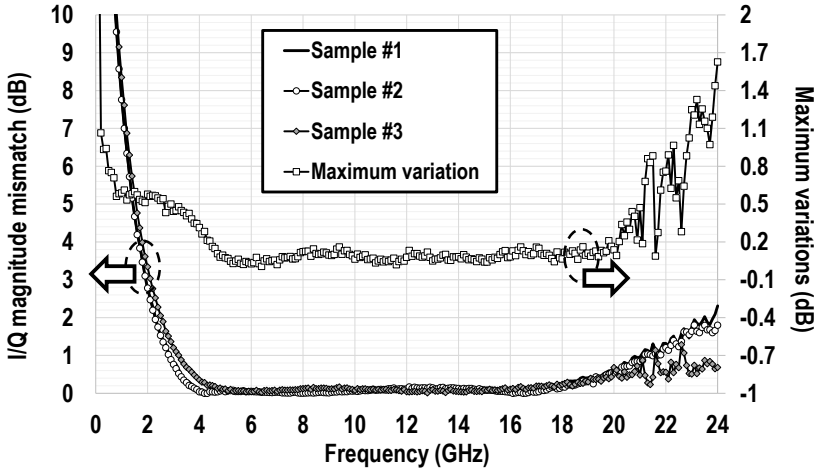
I/Q magnitude mismatch (dB)
Maximum variations (dB)
Sample #1
Sample #2
Sample #3
Maximum variation
Frequency (GHz)

(c)

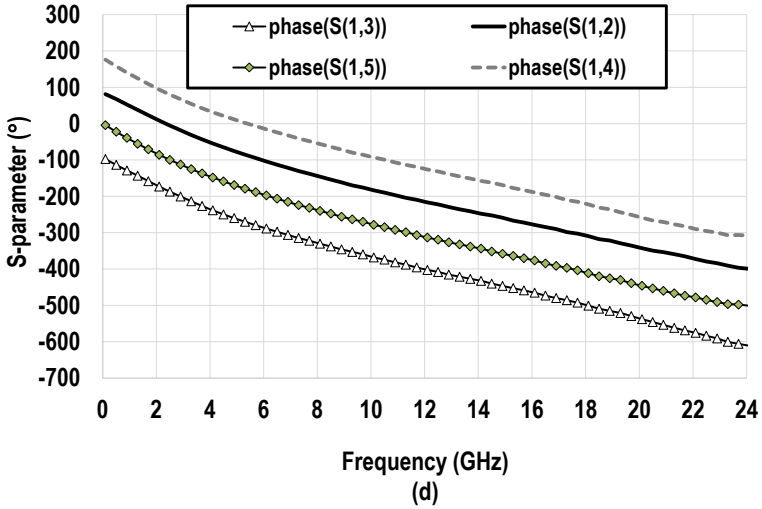
S-parameter (°)
phase(S(1,3))
phase(S(1,2))
phase(S(1,5))
phase(S(1,4))
Frequency (GHz)

(d)

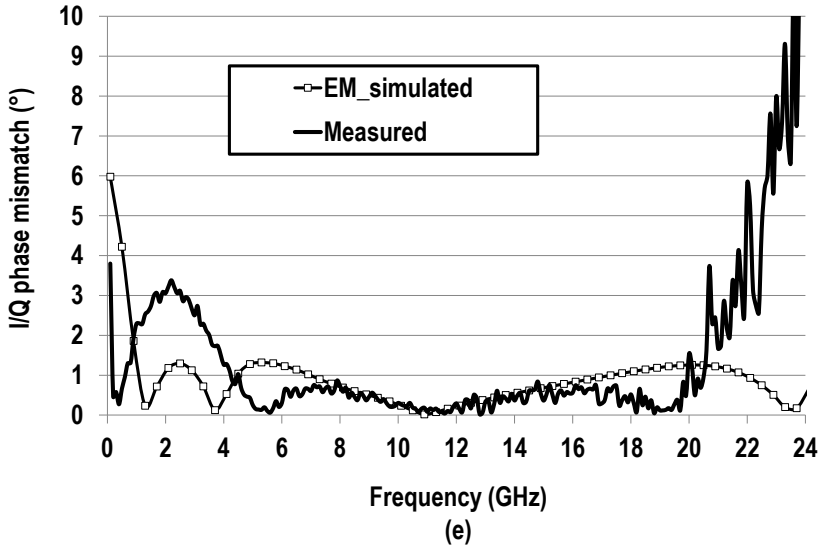
EM_simulated
Measured
I/Q phase mismatch (°)
Frequency (GHz)

(e)

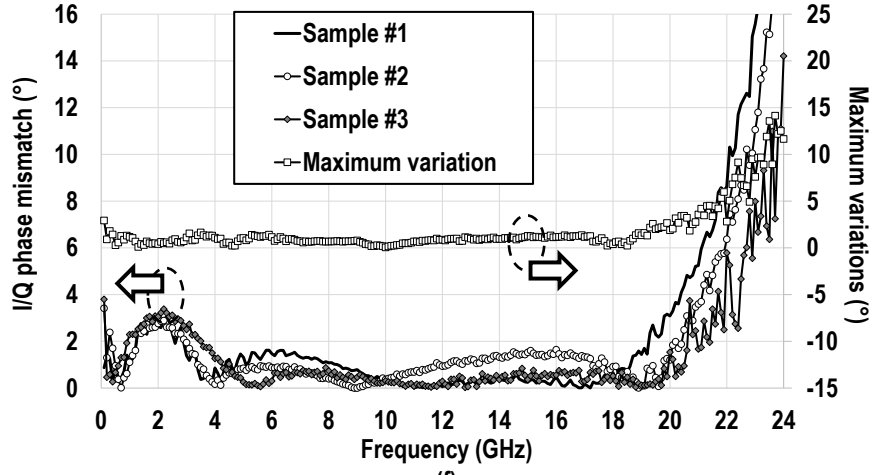
Sample #1
Sample #2
Sample #3
Maximum variation
I/Q phase mismatch (°)
Maximum variations (°)
Frequency (GHz)

(f)

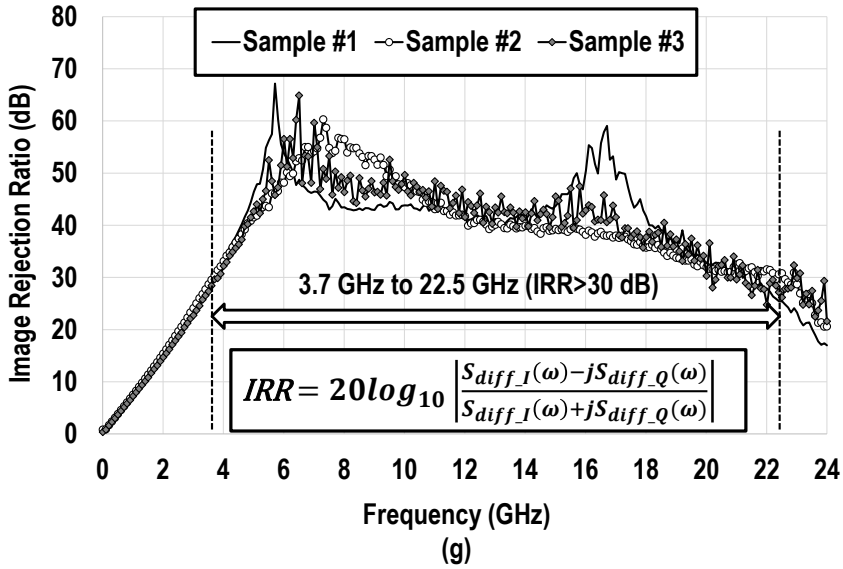
Sample #1
Sample #2
Sample #3
3.7 GHz to 22.5 GHz (IRR>30 dB)
$IRR = 20log_{10}\left|\frac{S_{diff\_I}(\omega) - jS_{diff\_Q}(\omega)}{S_{diff\_I}(\omega) + jS_{diff\_Q}(\omega)}\right|$
Image Rejection Ratio (dB)
Frequency (GHz)

(g)

Fig. 18. (a) Measured magnitudes response and (b) simulated, measured, and calculated I/Q magnitude mismatch of the 3-stage transformer poly-phase network. (c) Meausred I/Q magnitude mismatches of 3 independent samples. One differential 100 Ω input and four single-ended 50 Ω outputs are used for (a), (b) and (c). (d) Measured phases and (e) measured and EM simulated output I/Q phase mismatch. (f) Meausred I/Q phase mismatches of 3 independent samples. (g) The calculated IRR based on the measured 3 independent samples. The port definitions are shown in Fig. 16.

Figure 18(a) shows the typical s-parameter measurements of one sample. Since the theoretical loss of this passive network is 6 dB due to the 1:4 power splitting, the measured passive loss of the 3-stage transformer poly-phase network is only 3.65 dB at 6.4 GHz. The 3 dB magnitude bandwidth is from 2.3 GHz to 18 GHz. Both results closely match the 3D EM simulation results shown in Fig. 14(b). The measured input matching is below -10 dB from 0.5 GHz to 21.3 GHz.

The measured I/Q magnitude mismatch for one sample is within 1 dB from 2.9 GHz to 22.5 GHz. In Fig. 18(b), this measured result is compared with 3D EM simulation result and the calculated result based on theoretically derived close-form design equation (35). Close agreement is achieved among these three results. The slight difference between the calculated I/Q magnitude mismatch and measured I/Q magnitude mismatch is mainly due to the finite Q of the transformer and the micro-strip transmission line magnitude/phase offsets.

The measured I/Q magnitude mismatch results for all the 3 independent CMOS samples are summarized in Fig. 18(c). An ultra-wide bandwidth is consistently achieved, showing the robustness of the proposed transformer-based poly-phase network design. The maximum variation of I/Q magnitude mismatch of independent 3 samples from 2.9 GHz to 21 GHz is below 0.5 dB. The measured maximum variation of the passive loss of independent 3 samples is 0.3 dB with the average passive loss of 3.65 dB at 6.4 GHz.

Next, the typical measured differential output quadrature phase responses are shown in Fig. 18(d). The measured differential I/Q phase mismatch is compared with the

3D EM simulation in Fig. 18(e). This measured maximum I/Q phase imbalance is within 10° from low-frequency up to 24 GHz. The measured I/Q phase mismatch matches well with 3D EM simulation up to 20 GHz, and the slightly smaller bandwidth of the measured phase result is mainly due to the additional parasitic capacitances in practice. The measured phase mismatches of the 3 independent CMOS chip samples are summarized in Fig. 18(f). The maximum variation of I/Q phase mismatch of independent 3 samples from 0.1 GHz to 21.5 GHz is below 5°, also showing the robustness of the proposed transformer-based poly-phase network design. The Image Rejection Ratio (IRR) is often used to evaluate the quality of the quadrature signals to include both I/Q magnitude and phase mismatches [4] [18]. The IRR can be defined as,

$$\mathrm{IRR} = 20\log_{10}\left|\frac{S_{\mathrm{diff_I}}(\omega) - jS_{\mathrm{diff_Q}}(\omega)}{S_{\mathrm{diff_I}}(\omega) + jS_{\mathrm{diff_Q}}(\omega)}\right| \tag{46}$$

Figure 18(g) shows the calculated image rejection ratio based on the measured 3 independent CMOS chip samples. The calculated IRR is more than 30 dB from 3.7 GHz to 22.5 GHz with peak IRR of 67.2 dB at 5.71 GHz. For IRR>20 dB, I/Q magnitude mismatch and I/Q phase mismatch should be below 1 dB and 10°, respectively [18] and the calculated IRR is more than 20 dB from 2.7 GHz to 24 GHz.

In summary, these measurement results demonstrate that our proposed 3-stage transformer poly-phase network achieves high-quality quadrature signal generation with low-loss (3.65 dB at mid-band), a compact area, and a first-ever one-decade bandwidth. Note that such a low-loss and ultra-wideband quadrature generation cannot be achieved by conventional RC-CR poly-phase networks due to their severe signal losses in high-order implementations.

CHAPTER VI

CONCLUSION

In this paper, a transformer-based poly-phase network is proposed and demonstrated to achieve high-quality quadrature signal generation with low-loss, compact size, and an ultra-wide bandwidth. We first present a high-k transformer quadrature hybrid design with the complete circuit analysis and design equations. Such a high-k transformer quadrature hybrid achieves substantial size reduction and bandwidth extension compared with the convention transformer hybrid design with k=0.707. The I/Q magnitude and phase mismatches are also analyzed for high-k transformer hybrids with analytical equations. Next, we introduce the proposed multistage transformer-based poly-phase network by cascading multiple transformer poly-phase unit stages, which are based on the high-k transformer quadrature hybrids. The behavior of such multistage transformer-based poly-phase network is studied. In particular, the suppressions of the I/Q magnitude and phase mismatches by cascading multiple poly-phase stages are analyzed, formulated by close-form equations, and demonstrated based on simulations. As a proof-of-concept, a 3-stage transformer-based poly-phase network is implemented in a standard 65 nm bulk CMOS process with a core area of 772 μm×925 μm. Simulations based on the 3D EM modeling verify the high-precision and ultra-wideband quadrature generation of the proposed network and thus validate the theoretical analysis and the derived close-form design equations. The measured passive loss of the 3-stage poly-phase network is 3.65 dB at 6.4 GHz. The measured output I/Q magnitude mismatches is below 1 dB from 2.9 GHz to 22.5 GHz and the measured I/Q phase imbalance is lower than 10° from 0.1 GHz to 24 GHz. An effective Image-Rejection-Ratio (IRR) of more than 30 dB from 3.7 GHz to 22.5 GHz and more than 20 dB from 2.7 GHz to 24 GHz are achieved. The proof-of-concept 3-stage transformer-based poly-phase network design achieves high-quality quadrature generation with low loss and a first-ever one-decade bandwidth. Measurement results on 3

independent CMOS chip samples exhibit consistent performance and show the robustness of the proposed transformer-based poly-phase network design.

TABLE I
COMPARISON OF STATE-OF-THE-ART SILICON-BASED QUADRATURE GENERATION SCHEME

	Type	Frequency range	Loss	I/Q mag/phase error	Chip size	Input matching
This Work	**3-stage transformer-based poly-phase network**	**2.7 GHz to 24 GHz[1] 3.7 GHz to 22.5 GHz[2] 2.3 GHz to 18 GHz[3]**	**3.65 dB**	**1 dB/10° (IRR>20 dB)[1] 0.5 dB/2° (IRR>30 dB)[2] 2.5 dB/3.3°[3]**	**772×925 μm^2**	**100 Ω (differential)**
[10]	Single-ended transformer-based quadrature hybrid	1.95 GHz at 2.05 GHz	1.7 dB	IRR>30 dB	390×350 μm^2	50 Ω (single-ended)
[12]	Folded transformer-based quadrature hybrid	4.75 GHz to 5.41 GHz	0.82 dB	±0.5 dB/3.8°	260×260 μm^2	100 Ω (differential)
[13]	L-C resonance based quadrature all-pass filter	5.5 GHz to 17.5 GHz	N/A	2.4 dB/10°	430×160 μm^2	50 Ω (differential)
[17]	3-stage RC-CR poly-phase filter	2.5 GHz to 10 GHz	10 dB	IRR>35 dB	N/A	Not matched

1. IRR>20 dB bandwidth. 2. IRR>30 dB bandwidth. 3. 3 dB insertion loss bandwidth

REFERENCES

[1] J. Park, *et al*., "A K-band 5-bit digital linear phase rotator with folded transformer based ultra-compact quadrature generation," *IEEE Radio Frequency Integrated Circuits Symposium Dig.,* Jun. 2014, pp. 75-78.

[2] S. Hu, *et al.,* "A +27.3dBm transformer-based digital Doherty polar power amplifier fully integrated in bulk CMOS," *IEEE Radio Frequency Integrated Circuits Symposium Dig.,* Jun. 2014, pp. 235-238.

[3] D. M. Pozar, *Microwave Engineering*, 4th edition, Wiley, 2011.

[4] B. Razavi, *RF Microelectronics*, 2nd edition, Prentice Hall, 2012.

[5] J. Park, *et al*., "An ultra-broadband compact mm-wave butler matrix in CMOS for array-based MIMO systems," *IEEE Custom Integrated Circuit Conference Dig.,* Sept. 2013, pp. 1-4.

[6] S. Jeon, *et al*., "A scalable 6-to-18 GHz concurrent dual-band quad-beam phased-array receiver in CMOS," *IEEE J. Solid-State Circuits*, vol. 43, no. 12, pp. 2660-2673, Dec. 2008.

[7] C. Balanis, *Antenna Theory Analysis and Design*, Wiley, 2005.

[8] F. Behbahani, *et al*., "CMOS mixers and polyphase filters for large image rejection," *IEEE J. Solid-State Circuits*, vol. 36, no. 6, pp. 873-887, Jun. 2001.

[9] S. Kim, *et al*., "An improved wideband all-pass I/Q network for millimeter-wave phase shifters," *IEEE Transaction on Microwave Theory and Techniques*, vol. 60, no. 11, pp. 3431-3439, Nov. 2012.

[10] R. C. Frye, *et al.,* "A 2-GHz quadrature hybrid implemented in CMOS Technology," *IEEE J. Solid-State Circuits*, vol. 38, no. 3, pp. 550-555, Mar. 2003.

[11] M. Tabesh, *et al*., "60GHz low-loss compact phase shifters using a transformer-based hybrid in 65nm CMOS," *IEEE Custom Integrated Circuit Conference Dig.,* Sept. 2011, pp. 1-4.

[12] J. Park, *et al*., "A fully differential ultra-compact broadband transformer based quadrature generation scheme," *IEEE Custom Integrated Circuit Conference Dig*., Sept. 2013, pp. 1-4.

[13] K. Koh, *et al*., "An X- and Ku- band 8-element phased-array receiver in 0.18μm SiGe BICMOS technology," *IEEE J. Solid-State Circuits*, vol. 43, no. 6, pp. 1360-1371, Jun. 2008.

[14] R. Han, *et al*., "A 260GHz broadband source with 1.1mW continuous-wave radiated power and EIRP of 15.7dBm in 65nm CMOS," *IEEE International Solid-State Circuits Conference Dig.*, Feb. 2013, pp. 138-139.

[15] W. Cao, *et al*., "Multi-frequency and dual-mode patch antenna based on electromagnetic band-gap (EBG) structure," *IEEE transaction on Antennas and Propagation*, vol. 60, no. 12, pp. 6007-6012, Dec. 2012.

[16] J. Park, *et al*., "A Transformer-based poly-phase network for ultra-broadband quadrature signal generation," *IEEE MTT-S International Microwave Symposium (IMS)*, May. 2015.

[17] K. Stadius, *et al*., "Multitone fast frequency-hopping synthesizer for UWB radio," *IEEE Transaction on Microwave Theory and Techniques*, vol. 55, no. 8, pp. 1633-1641, Aug. 2007.

[18] W. Lin, *et al*., "1024-QAM high image rejection E-band sub-harmonic I/Q modulator and transmitter in 65-nm CMOS process," *IEEE Transaction on Microwave Theory and Techniques*, vol. 61, no. 11, pp. 3974-3985, Nov. 2013.